Flexible Barrier Materials for Improving the Durability of Photovoltaic Devices

Gabriella Rossi

Department of Industrial Engineering

Ph.D. Course in Chemical Engineering
(XII Cycle-New Series)

Flexible Barrier Materials for Improving the Durability of Photovoltaic Devices

Supervisors   **Ph.D. student**
Prof. Loredana Incarnato   *Gabriella Rossi*
Prof. Paola Scarfato

Scientific Referees
Prof. Paolo Ciambelli
Prof. Heinrich-Christoph Neitzert

Ph.D. Course Coordinator
Prof. Paolo Ciambelli

Dedicated to Susanna and Lorenzo

Acknowledgements

Publications

G. Rossi, C. Altavilla, P. Scarfato, P. Ciambelli and L. Incarnato, *"Deposition of transparent and flexible nanolayer barrier on standard coating materials for photovoltaic devices"*, Surface and Coatings Technology, Volume 239, 25 January 2014, Pages 200–205.

G. Rossi, P. Scarfato and L. Incarnato, *"Active Barrier Films of PET for Solar Cell Application: Processing and Characterization"*, 7th International Conference on Times of Polymers Composites, Ischia, Italy, 24-26 June 2014 (accepted).

G. Rossi, C. Altavilla, P. Scarfato, P. Ciambelli and L. Incarnato *"Nanolayers of alkylsilanes and fluoroalkylsilanes for improving the oxygen barrier properties of coating materials for solar cells"*, Proceedings of NANOTECH ITALY 2013, ISBN 978-88-6140-152-5, Venice 27-29 November 2013

G. Rossi, E. Avallone, M. R. Galdi, P. Scarfato and L. Incarnato, *"Active barrier coating for solar cells"*, European Conference on Smart & Functional Coatings, Turin, 26-27 September 2013

G. Rossi, C. Altavilla, , P. Scarfato, P. Ciambelli and L. Incarnato, *"Flexible and transparent multibarrier coating for solar cells"*, European Conference on Smart & Functional Coatings, Turin, 26-27 September 2013

G. Rossi, C. Altavilla, P. Scarfato, P. Ciambelli and L. Incarnato, *"Transparent and hydrophobic nanocoating materials for photovoltaic*

cells" Fuelling the Future: Advances in Science and Technologies for Energy Generation, Transmission and Storage (December 2012). Editor: A. Mendez-Vilas. Publisher: BrownWalker Press, pp. 271-275. ISBN-13: 978-1-61233-558-2.

G. Rossi, C. Altavilla, P. Scarfato, P. Ciambelli and L. Incarnato*"Materiali flessibili trasparenti ed idrofobici ottenuti tramite chemisorbimento di film nano-strutturati su PET silicizzato"* Atti del XI Convegno AIMAT, Gaeta, 16-19 September 2012, pp 455-458. ISBN 978-88-97930-037.

G. Rossi, C. Altavilla, P. Scarfato, P. Ciambelli and L. Incarnato, *"Transparent and hydrophobic nanocoating materials for photovoltaic cells"*, Book of Abstracts of The Energy & Materials Research Conference EMR 2012, Torremolinos, Spain, 20-22 June 2012 (oral presentation).

LIST OF CONTENTS

II

LIST OF FIGURES

V

LIST OF TABLES

VII

Abstract

The economic viability of photovoltaic (PV) devices is strongly dependent upon equipment cost and durability. During their usage, these devices are exposed to several atmospheric degradation agents and thus they need to be protected by coatings and encapsulants. However, even such coatings and encapsulants can degrade over time due to weather conditions, leading to potential efficiency loss and damage of the photovoltaic devices.

Nowadays, the following main properties are basically required for solar cells coating materials to ensure PV devices durability: UV, oxygen and water barrier; thermal stability, transparency, anti-reflectance, anti-soiling, flexibility, affordable cost, electrical isolation.

Therefore, in order to maintain a high efficiency during their lifetime solar cells require coating materials with several functions that are usually achieved with multilayer coatings, in which one or more layer have a specific functionality, such as gas and moisture barrier, liquid barrier and self-cleaning properties. However, a higher number of layers normally increases the cost and reduces the coating transparency and flexibility. A reduction of the number of layers would lower costs and also help to maintain a high transparency and flexibility.

This study was focused to the development of novel flexible and transparent materials able to integrate into a single layer both liquid and gas barrier functionalities by means of simple and effective single step process carried out at room temperature, specifically applied to standard coating bilayers for PV cells. To this aim, a Self Assembly of Monolayers of alkylsilanes and fluoroalkylsilanes was chemisorbed on the silica surface of a PV standard coating bilayers for solar cells such as PET-SiOx and ETFE-SiOx. The so obtained nanocoated films showed high hydrophobic characteristics with average contact angle higher than 130° for the coated PET-SiOx substrate, and a significant improvement of the oxygen barrier properties, reducing the Oxygen Transmission Rate to 1/3 if compared to that of the uncoated film.

Accelerate Ageing tests were performed in order to verify the chemical resistance of the nanocoated materials by simulating the degradation effect of both acidic and basic rains, damp heat, UV exposure. The measured contact angle values showed that after an initial slight reduction of the

contact angle value, a constant hydrophobic value was maintained for the samples coated with the SAM of fluoroalkylsilanes, even after 1000 hours of very drastic test conditions.

Therefore, the above nanocoated materials were compared to several multilayer structures that were laminated with uncoated PET-SiOx and ETFSiOx. It was found that the barrier properties of the nanocoated PETSiOx layer are higher than those of 2 PET-SiOx layers, thus confirming that the so improved barrier coating materials allow a reduction in the number of the necessary protective layers for the PV devices. Finally, these multilayer structures with different number of layers and compositions were applied to organic solar cells at lab scale in order to assess their effectiveness in preserving the PV devices efficiency.

Preliminary data have showed that the multilayer structure that include the nanocoated multi-barrier layer are more effective in protecting the solar cells than the other multilayer structures and that the efficiency values of the organic solar cells coated with our flexible multilayer after more than 70 days are comparable with those of solar cells encapsulated with glass.

Furthermore, another approach was pursued in this study in order to enhance the protective action of the passive barrier with the addition of an active barrier coating, able to continuously adapt its protective action according to the intensity of the environmental degradation phenomena. The driving idea is that of including in suitable polymer substrate specific oxygen absorbers, which are activated by meteorological phenomena (diurnal temperature variation, rain, etc.). To this aim active PET films were produced including an oxidizable phase that is activated by liquid water. The preliminary characterization results showed that these active barrier layers are suitable for coating photovoltaic cells, since their absorption kinetics is slow, they show an acceptable transparency and are proven to be easily processable.

Further research is still needed in order to study the effect of our passive and active barrier materials on the durability of the organic PV devices, as well as to optimize the multilayer structure design and the encapsulation process. The preliminary data on the active barrier layers are encouraging and represent a starting point for further study activities.

Chapter I
Durability issues for photovoltaic devices

I.1 Introduction

Photovoltaics[1] (PV) is a key technology option to realise the shift to a decarbonised energy supply. The solar resources in Europe and world-wide are abundant and cannot be monopolised by one country. Furthermore, photovoltaics and other renewable energies are the only ones to offer a reduction of prices, rather than an increase in the future.

From 2008 to second quarter of 2013, residential PV electricity system prices have decreased by almost 60% in the most competitive markets, and in some markets, the cost of PV-generated electricity is already cheaper than residential electricity retail prices. It is interesting to note that module prices decreased even more, by over 80%, during the same period and now represent less than 40% of the costs of a PV system. Due to falling PV system prices and increasing electricity prices, the number of such markets is steadily increasing. The consequences of the nuclear accident which took place in Fukujima in March 2011, was a shift in energy investments toward more renewables and photovoltaic systems. In 2012, solar energy attracted 57.7% of all new renewable energy investments or USD 137.7 billion (EUR 105.9 billion).

After the world-wide photovoltaic market more than doubled in 2010, the market grew again by almost 30% in 2011. In 2012, PV industry production increased again but more modestly than previous years, increasing by around 10% and reaching a worldwide production volume of about 38.5 GWp of photovoltaic modules. The PV sector is still a growing sector in spite of the financial crisis. The compound annual growth rate over the last decade was

---

[1] Source: European Commission - Joint Research Centre - Institute for Energy and Transport. PV Status Report 2013.

about 55%, which makes photovoltaics one of the fastest growing industries at present.

There are two leading manufactured solar photovoltaic technologies in commercial use today: crystalline silicon PV and thin film PV. The vast majority of solar module demand comes from crystalline silicon (80%) with thin-film making up the balance. Since 2008, thin film has gained ground on crystalline silicon largely due to the higher manufacturing costs associated with crystalline silicon PV. Thin-film PV is the fastest growing sector of the solar cell manufacturing industry.

Thin-film cells are manufactured by applying very thin layers of semiconductor material to inexpensive materials such as glass, plastic or metal. Thin-film semiconductors absorb light more easily than c-Si, therefore requiring less semiconductor material, making them far less expensive than crystalline silicon modules. There are three main typologies of thin-film PV modules presently:

- CdTe or Cadmium Telluride thin-film,
- a-Si or Amorphous Silicon thin-film,
- CIGS or Copper Indium Gallium Selenide thin-film.

Organic photovoltaic devices (OPVs), employing organic conductive polymers, are also to be mentioned for their potential to become a low-cost alternative to solid-state solar cells. Research into OPVs is rapidly growing worldwide because it offers a route to low temperature, inexpensive processing of lightweight, flexible solar cells that can be mass manufactured cheaply.

I.2 Durability of photovoltaic devices

Increasing the durability of photovoltaic (PV) plants at an acceptable cost is becoming one of the most challenging issue to foster the diffusion of PV. For instance, stringent requirements for PV modules life time of at least 30 years have been delivered by the US Department of Energy. One of the most important technological factors to enhance the PV modules durability is represented by the availability of suitable coating materials with high barrier properties, flexibility, and affordable cost.

Different PV systems (c-Si, thin film, organic PV) have different modules lifetime, with the higher module lifetime corresponding to the most mature technology and the lower values to the latest technologies.

Crystalline Silicon Cells commercially available are generally guaranteed for 25-30 years, while for instance 2-3 years is the guaranteed operational lifetime for commercially available flexible CIGS solar cells and even lower lifetimes can be measured for polymer solar cells. Therefore, the barrier properties of coating materials are of a special concern for thin film PV cells,

2

which are more sensitive against the degradation effect due to atmospheric agents.

Indeed, although crystalline silicon panels are the oldest, most reliable and highly efficient PV panels in the market today, they still present durability issues that need to be tackled.

Information on PV module (wafer-based) degradation has been collected since the early 1970's, but the work seems to be inadequately coordinated. Power degradation rates for c-Si modules between 0.7% and 9.8% in the first year and between 0.7% and 4.9% in the second year have been reported[2]. A recent study of Abenante et al. (2010) was carried out at the experimental station of ENEA for measuring the efficiency degradation over a 30 years period providing the following results:

- current average efficiency: 8,3% (87% of the initial value);
- absolute efficiency decrease of 1,2% in 30 years;
- total relative efficiency decrease of 13%.
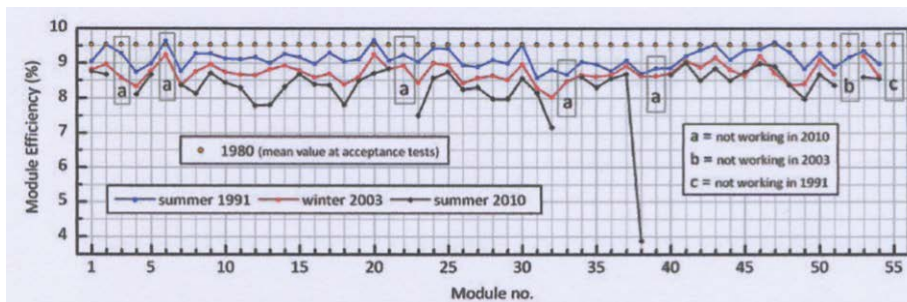
Figure I.1 *Comparison of modules efficiency in years 2010, 2003 and 1990.*

The operational module lifetime is generally defined as the period in which its power output decreases by less than 20%. What is usually referred to in photovoltaics as "reliability," such as no more than 1% power loss per year to a maximum of 20%, is actually a durability issue.

The efficiency reduction of the PV modules is caused by several and different degradation mechanisms that will be briefly examined in the following section. One of the most important technological factor to be considered for enhancing the PV modules life time is represented by the

---

[2] LEEETISO,CH-Testing Centre for Photovoltaic Modules,
http://leee.dct.supsi.ch/PV/Results/Tested_modules.htm

availability of suitable encapsulant and coating materials with high barrier properties, flexibility and affordable cost.

In particular (Erler et al., 2003), modules based on thin film solar cells are significantly more sensitive against the degradation effect of the atmospheric agents than modules using crystalline Si-solar cells and the demands on encapsulation materials are much higher for thin film solar cells.

The degradation of the PV devices that leads to durability and reliability problems is caused by several factors.

The use of the words reliability and durability are not consistent throughout the literature. To avoid confusion the word durability will be used in connection with the slow, gradual, time-dependent performance loss in a PV cell, module, or system, while the term reliability will be used to describe sudden failures.

General reliability issues across all PV technologies are (Bosco, 2010):

- corrosion leading to a loss of grounding,
- quick connector reliability,
- improper insulation leading to loss of grounding,
- delamination,
- glass fracture,
- bypass diode failure,
- inverter reliability,
- moisture ingress.

In addition, there are issues specific to the individual technologies, to name a few:

i. wafer silicon: light-induced cell degradation, front surface soiling, effect of glass on encapsulation performance, reduced adhesion leading to corrosion and/or delamination, busbar adhesion degradation, junction box failure;

ii. thin film silicon: electrochemical corrosion of SnO2, initial light degradation;

iii. CdTe: interlayer adhesion and delamination, electrochemical corrosion of SnO_2:F, shunt hot spots at scribe lines before and after stress;

iv. CIS: interlayer adhesion, busbar mechanical adhesion and electrical, notable sensitivity of TCO to moisture, moisture ingress failure of package;

v. OPV: photolytic instability, moisture induced degradation, moisture ingress failure of package.

Another study (Quintana et al. 2002) classifies the degradation phenomena of the PV modules into five categories that ultimately drive performance loss and possibly failure. These are:

4

1) degradation of packaging materials,
2) loss of adhesion,
3) degradation of cell/module interconnects,
4) degradation caused by moisture intrusion,
5) degradation of the semiconductor device.

Degradation of encapsulant and packaging materials

Module package degradation occurs when the laminate package is damaged or packaging materials degrade during normal service, affecting the function and/or integrity of the module. Examples of packaging degradation include glass breakage, dielectric breakdown, bypass diode failure, encapsulant discoloration, and backsheet cracking and/or delamination. Package degradation can cause module performance failures, which can lead to system level issues like array performance failure, safety hazards, and/or failure of a supplemental function, e.g. a module functioning as a window in a BIPV application.

Loss of adhesion

Delamination is defined as the breakdown of the bonds between material layers that constitute a module laminate.

Field experience has shown that front-side delamination at the glass/encapsulant and cell/encapsulant interfaces is more common than backside delamination. Front-side delamination causes optical decoupling of materials that transmit sunlight to the cells, resulting in performance degradation. Delamination on either side interrupts efficient heat dissipation and increases the possibility of reverse-bias cell heating. Higher cell operating temperatures cause performance degradation.

Degradation of cell/module interconnects

Interconnect degradation in crystalline silicon modules occurs when the joined cell-to-ribbon or ribbon-to-ribbon area changes in structure or geometry. "Coarsening", a change in joint structure, occurs as a result of segregation of the metals (SnPb) in the soldering alloy. Coarsening causes the formation of larger metal grains that undergo thermomechanical fatigue, enhancing the possibility of cracking at the grain boundaries and possible joint failure.

Interconnect degradation in thin-film modules is distinctively different. Observations of field-aged modules have found that a prime location for continuity failure is the point where the junction-box interconnect strap bonds to the cell frit. This is a very vulnerable solder bond that is likely to incur thermomechanical fatigue as a result of daily thermal cycling. Thin-film module scribe-line problems emerge when either the SnO_2 cell isolation scribe-lines or the back metal cell isolation scribe lines do not have the

5

material completely removed. In either case, partially shunted cells are the result.

Degradation caused by moisture intrusion

Moisture permeation through the module backsheet or through edges of module laminates causes corrosion and increases leakage currents. Corrosion attacks cell metallization in crystalline silicon modules and semiconductor layers in thin-film modules, causing loss of electrical performance. Figure I.2 shows moisture-induced corrosion that caused gridline adhesion to the silicon cell to fail. Retention of moisture in module packaging materials increases material electrical conductivity. This causes increased leakage current and subsequent performance loss. Moisture intrusion has also been linked to loss of adhesional strength at bond interfaces in the module laminate. Moisture intrusion combined with damaged module packaging materials can introduce severe safety concerns in high voltage applications.
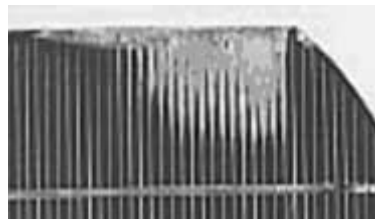
Figure I.2 *Moisture induced corrosion that caused bonds between the grid lines and the cell to fail.*

Degradation of the semiconductor device

Degradation of the semi-conductor material itself can also contribute to performance loss in field-aged modules. Crystalline silicon modules now have a long track record of performance stability in the field. This stability, in part, is due to the stability of the semiconductor material (crystalline silicon) used to make the cells. Field experience has indicated that the primary causes for performance loss in these modules have been associated with mechanisms external to the cells such as solder bonds, encapsulant browning, delamination and interconnect issues. Initial light induced degradation (LID) is one of the few changes that can be attributed to the c-Si semiconductor device. The LID effect is limited to the first few hours of outdoor module exposure and results in a 1-5% loss in short-circuit current (Saitoh et al. 2000).

It is also to be mentioned the Czochralski silicon (Cz-Si) specific lifetime degradation, that is induced by carrier injection or illumination. After an

6

illumination of about 12 h AM[3] 1.5 (depending on the doping level), the lifetime is reduced exponentially to a (fortunately) stable end value. This lifetime degradation can be completely reversed by an anneal step of around 200 8C in room ambient. This phenomenon is very similar to the Staebler–Wronski effect in amorphous solar cells and was related to the presence of interstitial oxygen in the Cz-Si grown crystals (Goetzberger et al. 2003).

Another form of degradation in crystalline cells is a result of chemically assisted diffusion of cell dopant (phosphorous) to the cell surface. High concentrations of phosphorous, along with sodium migrating from soda lime glass superstrates to the cell surface, have always correlated to low adhesional strength at the cell/encapsulant interface. Furthermore, it has been reported that loss of adhesional strength is exacerbated by exposure to high humidity environments (Dhere 2000, Dhere 2001).

Degradation and/or stabilization of a-Si modules have been the subject of many studies but there seems to be a lack of complete understanding of the mechanisms and environmental influences that cause performance degradation, such as the initial light induced degradation (Staebler–Wronski effect) (King et al. 2000, Wronski, 2000).

Recent data from fielded CdTe and CIS applications suggests higher than expected performance degradation and potential for system level failures.

Damp heat studies (Olsen et al.) of CIGSS and CdTe cells have been conducted by subjecting cells and min-modules to an environment 60C/90%RH, showing that both CIGSS and CdTe cells degrade rapidly under 60C/90%RH unless they are protected with a barrier coating.

---

[3] AM: Air Mass

7
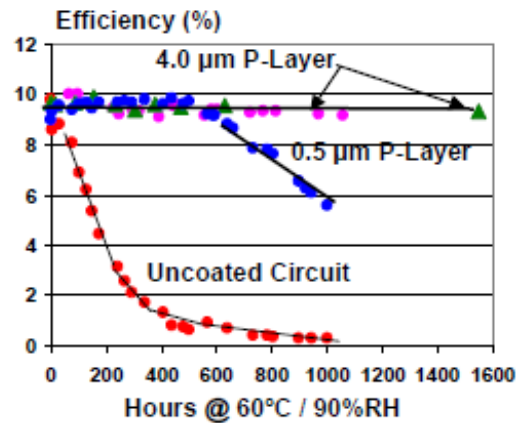
Figure I.3 *Efficiency versus time for three encapsulated min-modules and one uncoated CIGSS circuit.*

As for the organic PV devices, the degradation mechanisms of conjugated polymer materials used in these cells were also studied (Krebs and Norrman 2007). It was found that molecular oxygen diffuses into the device causing oxygen-containing species to be generated throughout the active layers.

Conjugated (Lungenschmieda et al. 2006) polymers are known to be rather unstable in air, being particularly susceptible to photodegradation induced by oxygen and moisture. Especially poly(p-phenylene vinylene) (PPV) and its derivatives are susceptible to degradation in atmosphere. The mechanism involves the binding of oxygen atoms to vinyl bonds, which breaks the conjugation and leads to the formation of carbonyl groups. Besides, it has been reported that water can affect the interface between the metallic contact and organic semiconductors by an electrochemical process that causes delamination of the electrode.

I.3 Degradation of encapsulant and coating materials

The wafer-based PV devices are generally encapsulated with EVA with a front layer of glass and a backsheet of tedlar. Sometimes, for particular needs (such as BIPV), transparent PV modules are glass-EVA-glass laminated. Recently, also silicone has been studied and proposed as an alternative to the EVA encapsulants. An example of commercial product is the SilTRUST* transparent silicone encapsulant material presented from Momentive Performance Materials Inc at the Polymers in Photovoltaics 2012 forum in Cologne.

However, in practice glass is still the only frontsheet material used for wafer-based PV modules.

8

Thin film solar cells are generally encapsulated with glass or multilayer flexible films comprising different layers and also including high barrier layer(s). For instance, CIGS modules are encapsulated using vacuum lamination or roll to roll lamination of the gas barrier material (glass or barrier foil) with encapsulating materials as EVA, silicons or other encapsulant. Lateral permeation from the edge is difficult to control due to poor intrinsic gas barrier properties of encapsulating polymers and delamination process occurring with aging.

In general, the coating and encapsulant materials degradation can be of the following types: thermal, oxidative, photoinduced, mechanochemical, chemical, metal-catalyzed, and combinations of these (Czanderna and Pern 1996, Quintana et al. 2002).

Furthermore, also soil (e.g. dust, limestone, etc.) deposition (Hammond et al. 1997) on the frontsheet surface can reduce the coating transparency and, as a consequence, the efficiency of PV devices.

In general, three main degradation causes can be identified for the encapsulant materials:
- UV radiations
- O_2
- H_2O.

Ultraviolet irradiation (Czanderna and Pern 1996) of polymers can bring about two primary types of reactions, chain scission and crosslinking. With sufficient exposure to either long-term moderate irradiation or short-term intensive irradiation, both these reactions will eventually result in changes in the mechanical properties of the polymers.
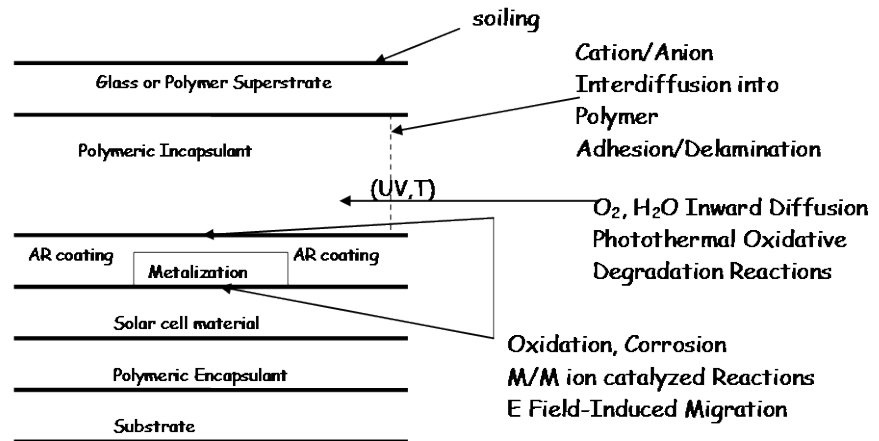
Fig. I.4 *Schematic cross-section of an encapsulated PV cell and relevant reactions/processes that may reduce the cell performance and/or service lifetime.*

Chain scission reactions lead to a reduction in the molecular weight of the polymer, eventually causing a loss in mechanical properties, since the ultimate mechanical properties such as elongation to break are usually very sensitive to a reduction in molecular weight.

Crosslinking reactions increase the stiffness of the polymer but also result in a decrease in the elongation to break. High levels of crosslinking will lead to enbrittlement of the polymer, which is particularly important for rubbery polymers used as adhesive or sealants. Crosslinking of rubbery polymers can decrease the ability of a polymer to recover from cyclic stress.

The permeability of polymers is influenced by both the mobility of the polymer chains and the strength of the interaction between the polymer and penetrant. The mobility of the polymer chains can be affected by prolonged exposure to environmental stresses.

The rate of permeation of gases through glassy polymers increases with increasing temperature, and is less sensitive to changes in temperature through rubbery polymers. Migration of plasticizer and stabilizers through glassy polymers is accelerated by increases in temperature. For hydrophilic polymers, an increase in the relative humidity can result in an increase in the permeability of both water vapor and other permeant gases.

Chain scission or crosslinking caused by UV irradiation can have a substantial influence on permeability. Chain scission increases the free

volume of the polymer system, which can lead to an increase in permeability. Crosslinking restricts the mobility of the polymer chains, which generally leads to a decrease in permeability.

Chapter II
Barrier materials for enhancing the durability of solar cells

II.1 Introduction

Nowadays, the following main properties are basically required for solar cells coating materials to ensure PV devices durability: UV, oxygen and water barrier (Morlier et al. 2013); thermal stability, transparency, anti-reflectance (Lu et al. 2011), anti-soiling, flexibility, affordable cost, electrical isolation (Frach et al. 2008). Some of these properties are competitive ones. For instance, high barrier properties may be achieved by increasing the number of coating layers (Logothetidis et al. 2010). However, a higher number of layers normally increases the cost and reduces the coating transparency and flexibility (Erler et al. 2003).

In order to maintain a high efficiency during their lifetime solar cells require coating materials with several functions that are usually achieved with multilayer coatings (Vaško et al. 2009, Visser 2008), in which one or more layer have a specific functionality, such as gas and moisture barrier (Jorgensen et al. 2006, Langereis et al. 2006), liquid barrier and self-cleaning properties (Karunakaran et al. 2011). A reduction of the number of layers would lower costs and also help to maintain a high transparency and flexibility.

II.2 Coating Materials with gas barrier properties

The ability of oxygen and moisture to cross an encapsulating membrane is expressed by the oxygen transmission rate (OTR) and the water vapor transmission rate (WVTR), respectively. It has been demonstrated and is generally accepted (Lungenschmied et al. 2006) that the lifetime of thin film

and organic PV cells require $10^{-4} \sim 10^{-3}$ g m^{-2} d^{-1} values of WVTR and 10^{-3} cm^3 m^{-2}d^{-1} atm^{-1} values of OTR (Fig. II.1) .
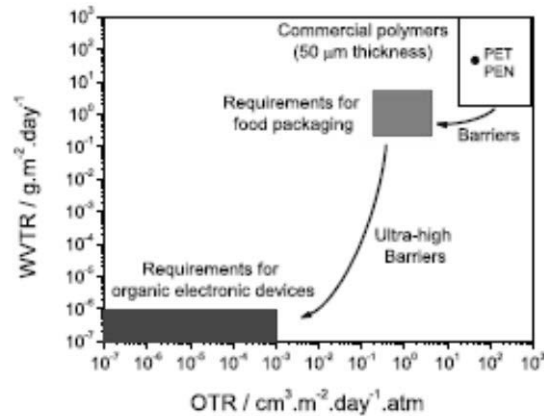
Figure II.1 *Water vapor transmission rate (WVTR) versus oxygen transmission rate (OTR) for commercial polymers, encapsulations required for food packaging and for organic electronics purposes.*

Thin film barrier coatings against permeation of gases and vapors deposited onto flexible polymer substrates have been intensively studied (Lungenschmied et al. 2006) for applications in food and pharmaceutical packaging, where improving the barrier capabilities of the bare plastic films by one to three orders of magnitude is usually considered sufficient.

The barrier protective films that are currently studied for the PV applications are generally composed of one or more layers of polymer substrate with an inorganic coating. The inorganic coating is generally consisting of SiOx or AlOx while the polymer substrate may be EVA, ETFE, PET or PEN. The inorganic coating is typically realised by PECVD or Electon Beam Evaporation, although, as already said before, more recent techniques like the ALD seem to produce higher quality of the coating (Langereis et al. 2006).

Because the moisture permeation properties of a single layer barrier are eventually limited by the defect density of the layer, the deposition of multilayer structures is expected to be the path towards the WVTR requirements mentioned above. Of course, the multilayer structures become most effective when the individual layers themselves have excellent permeation properties.

An example of a commercial multilayer material with very good barrier properties (WVTR ~10^{-6} g/m^{2}d) is the "**BARIX" film** of Vitex. It is composed of 4 bilayers polymer/inorganic. The Multilayer effectiveness is

14

based on two main factors: 1) redundancy and 2) tortuosity. In fact, the barrier response of the inorganic coatings is defined by their lattice disorder that results from the deposition process. This disorder has the form of macro- and nano-defects (pinholes and micro-cracks) that are formed during the growth process of the inorganic thin films by physical vapour deposition methods such as sputtering and evaporation.

These defects provide easy pathways for moisture and oxygen permeation, thus limiting the barrier performance of the inorganic film/polymer substrate system (Logothetidis et al. 2010). Therefore, the barrier mechanism is essentially due to a lag time effect[4]. However, the BARIX Film presents the disadvantage of a high cost, as a consequence of its complex production process that foresees several steps.

Other alternative approaches that have been developed for the gas barrier coating are:

- **Hybrid polymer ORMOCER® coating**: Sol-gel based processing of hybrid polymers (ORMOCER®s) with inorganic and organic structural units is used for functionalized coatings on a variety of substrates (ceramics, metals, polymers, etc). At temperatures below 150 °C the formation of both inorganic and organic network structures is possible. Functional organic groups bound to the inorganic network are used to modify surface properties. ORMOCER®-lacquers can be processed by all conventional coating techniques (dipping, spraying, spin on etc.) and cured by thermal or radiation energy. The dense inorganic network of ORMOCER®s combined with organic crosslinking and the possibility to control the polarity of the matrix, makes them useful as barrier layers for gases, vapors and ions (Haas et al. 1999). The introduction of functionalized alkoxides into thermally curable ORMOCER® systems can modify the coating surfaces. Hydrophilic/-phobic and oleophilic/-phobic can be achieved by the incorporation of appropriate functional groups. The wetting angles for water on fluorosilane modified ORMOCER® is > 110°.

- **Use of nanoparticles included in the inorganic layers**: this method allows to reduce the total number of layers. Several research works have investigated the use of nanoparticles in organic or inorganic layers. The (Ravichandran et al. 2008) use of a novel Saran (a co-polymer of vinylidene chloride and acrylonitrile) based polymer nanotube composite, which shows high transparency in the visible region, good barrier properties and thermal stability, has been studied for the encapsulation of OPV devices. Moreover, the inclusion of silicon dioxide particles has been studied in order to

---

[4] Source: Vitex Systems

further improve the barrier properties of the hybrid polymers. This method offers a possibility to increase the inorganic network degree of the ORMOCER® based polymers and thus should lead to a reduction of the OTR and WVTR values (Logothetidis et al. 2010). A commercial product that uses the nanoparticle in organic layers, in order to "seal" the defects of the inorganic layers. This approach allows to obtain a WVTR = 10^{-6} g.m^{-2}.d^{-1} and also of 10^{-4}. The nanoparticle increase surface area so that the residual moisture or oxygen can be effectively adsorbed and reacted with nanoparticles

- **Atomic Layer Deposition (ALD)**. The ALD technique has been studied to produce gas-diffusion barriers on polymers, and water vapour transmission rate of the order of $<0.5*10^{-4}$ g m^{-2}d^{-1} was reported for less than 15-nm thick Al_2O_3 depositions on polymers (Garcia et al. 2010a). Direct encapsulation of CIGS solar cells by ALD has also been shown to provide excellent stability in damp-heat conditions (Garcia et al. 2010b). However, since thin-film solar PV modules are rather protected by lamination than direct encapsulation, means to produce ALD ultra barriers by roll-to-roll process have been studied (Maydannik et al. 2011). Although ALD allows obtaining very dense layers with improved barrier properties, challenges still remain in implementing ALD for solar cell barriers. Robustness of the process towards cleanliness and surface chemistry of incoming substrates must be improved by pre-treatment processes. For example, planarization of the solar cell surface prior to the ALD process may offset a potential particle issue and provide chemically uniform surface with good adhesion to the thin-film barrier layer.

Concerning the commercial products, it is to be considered the current emergence on the market of new barrier films with medium barrier properties (Mitsubishi X Barrier, 3M Ultrabarrier solar film, Toppan, Amcor..etc). Other commercial products recently developed is the ENLIGHTTM Polyolefin Back Encapsulant Composite Films, a new polyolefin-based technology introduced by Dow Chemical that uses patent-pending technology to create a single structure that provides "2-in-1" functionality, serving as both the back encapsulant and backsheet for solar panels. However, it remains opaque and cannot be used as a front sheet.

A recent patent (Ichimura et al. 2012) that may be mentioned here to conclude this sub-section concerns a solar-cell back-side protective sheet for protecting solar modules from adverse weather conditions that could damage electrical insulation. The backsheet is provided with: a base film comprising at least one layer; a vapor-deposited film that is formed on the surface of the

16

base film and exhibits good barrier performance; and a coating layer that comprises at least one layer and is formed on the surface of the vapor-deposited film opposite the base film. Said coating layer is a ternary-copolymer layer obtained by curing a liquid film that has a resin component comprising a metal alkoxide with a reactive functional group (Y); an acrylic monomer with a reactive functional group (X) that reacts with the aforementioned reactive functional group (Y); and an acrylic monomer that does not have said reactive functional group (X).The proposed structures maintained good water vapour barrier properties (0,01 g/m^2 in 24 hours for a multilayered structure with a 75 µm PET layer, 5 µm of alkoxysilane adhesive, 12 µm of PET with silicon-dioxide vapour-deposited film, sandwiched between two layers of a 20 µm ternary copolymer) also after weathering tests.

II.3 Coating materials with liquid barrier properties

There are several methods for obtaining hydrophobic or superhydrophobic surfaces. In general, these methods try to imitate the hydrophobic mechanism which can be observed on natural objects such as the lotus leaf (the so called "lotus effect").

One of these methods for obtaining hydrophobic surfaces is represented by the Self Assembly of Monolayers (SAM) using precursor molecules with high hydrophobic properties in order to create protective nano-coatings. In particular, this method was applied by means of alkylsilanes and (fluoro)alkylsilanes deposition on glass substrates (Altavilla et al. 2011) and successfully allowed to obtain hydrophobic surfaces. Other methods that are employed to achieve superhydrophobicity are based on the introduction of a two-scale roughness (micrometric and nanometric scales), together with chemical functionalization.

An example is provided by the superhydrophobic and low light reflectivity silicon surfaces prepared by (Au)-assisted etching to form nanoscale roughness and thereby form hierarchical structures by metal-assisted etching of micron-size pyramid textured surfaces (Xiu et al. 2008), followed by surface fluorination with perfluorooctyltrichlorosilane (PFOS), and by a heat treatment at 150 ° C to complete the hydrophobic surface modification.

Moreover, it is worth mentioning the use of nanoparticles (NPs) that has been imposing as an effective way to control the surface nanoroughness. A simple approach was recently demonstrated by dip-coating a single layer of 60 nm SiO_2 NPs onto an amine-terminated self-assembled monolayer (SAM)-coated glass/silicon oxide substrate, followed by perfluorosilane deposition (Ling et al. 2009).

Another method (Karunakaran et al. 2011), that was proposed for creating transparent and superhydrophobic surface suitable for solar cells

17

applications, is based on the coassembly of amine-functionalized silica NPs (McConnell et al. 2009) of two different sizes (100 and 20 nm) followed by perfluorosilane deposition. This study (Karunakaran et al. 2011) allows to obtain very high hydrophobic properties and is applied on different substrates (glass, silicon, polyester materials). However, it is a multi-step process involving plasma treatment steps of the substrate surfaces as well as high temperature steps (>150 °C).

Although the above described approaches report very interesting results in terms of achieved hydrophobicity on substrates potentially applicable to the solar cells sector, they are likely to turn out to be expensive and difficult to be implemented at industrial level because they are multi-step processes, including complex and high temperature steps.

There is the need of a simple and single step process for obtaining hydrophobic surfaces suitable for the solar cells coating materials in order to improve the solar cells protection at affordable costs.

II.4 Coating Materials with active barrier properties

The passive barrier layers can be further improved by the combination with active oxygen barrier layers which have been developed for the food packaging industry (Amberg-Schwab et al. 2006). This approach makes these multilayer laminates promising candidates for special applications in the food packaging industry as well as for sophisticated applications in technical areas such as the encapsulation of sensitive organic devices like solar cells, organic light emitting diodes, or polymer electronic systems.

There are only few theoretical studies considering the use of suitable oxygen scavengers to be included in polymer barrier layers for solar cells.

An interesting research work (Amberg-Schwab et al. 2006) is based on the functional principle of the newly developed oxygen scavenger system, based on a photo-initiated, metal catalyzed oxidation of a cyclo-olefin bonded chemically to a silicate backbone. This concept permits the activation of the scavenging process by UV light and prevents the formation of low-molecular oxidation products which may decrease the quality of the packaged goods or may be toxic. The oxygen scavengers studied in this work are selected on the basis of two related patents of Chevron Chemical Company (Ching et al. WO99/48963) and Cryovac Inc (Matthews and Depree 2001) concerning the "Oxygen scavengers with reduced oxidation products for use in plastic films".

However, the PV cells have different technical requirements with respect to the food products, since the oxygen scavenging activity should be extended during the time, their transparency is to be maintained and the development of toxic by-products inside the solar module is not a problem so relevant as for the food industry.

18

Furthermore, SAES Getters[5] recently introduced some products with active barrier properties for water vapor such as: B-dry (edge sealant), DryPaste and AqvaDry (getter pastes), eDry (printable scavenger) and ZetaFill (printable active scavenger for OPV). Nevertheless, these products need to be stored in nitrogen atmosphere and at low temperature before they are applied and also have some drawbacks concerning the optical properties.

II.5 Aim of the study and structure of the PhD work

This Ph.D study aims to develop new passive and active barrier materials for coating flexible solar cells in order to extend their lifetime. The research objective is to study a simple method able to enhance the barrier properties against the atmospheric degradation agents of the flexible coating layers usually employed for coating solar cells. The final aim is to guarantee a higher protection degree with a lower number of coating layers, so reducing the material costs and increasing at the same time the flexibility and the transparency.

The research approach was focused on the study and development of novel flexible and transparent nanocoating, able to integrate into a single layer both liquid and gas barrier functionalities.

A simple and effective single step process carried out at room temperature was studied to apply a **<u>flexible passive multi-barrier coating with improved performance</u>** to standard coating bilayers usually employed for PV cells. The improved barrier properties against oxygen and liquid atmospheric agents are expected to guarantee higher lifetime for PV modules with higher flexibility and transparency and at lower costs.

In fact, although the related works (Karunakaran et al. 2011, Xiu et al. 2008, Ling et al. 2009, McConnell et al 2009, Teshima et al. 2003) report very interesting results in terms of achieved hydrophobicity on substrates potentially applicable to the solar cells sector, they are likely to turn out to be expensive and difficult to be implemented at an industrial level because they are based on multi-step processes, including plasma treatment and high temperature steps.

Thus, the novelty of the proposed approach consists in the study of a single step and room temperature process. Furthermore, both gas and liquid barrier properties of the modified surfaces were not investigated in the literature except for the study of Teshima et al. (2003), to our knowledge. However, the optical transparency properties were not analyzed in that study and the obtained performances in terms of gas (O_2) and liquid barrier improvement were too moderate to be considered of interest for PV applications.

---

[5] www.saesgetters.com

Subsequently, accelerate ageing tests were performed on the developed flexible multibarrier materials in order to assess the resistance of the barrier nanocoating in different conditions (damp heat, dipping cycles in varying pH solutions, UV exposure).

Finally, the encapsulation of organic solar cells with several flexible multilayer structures previously characterized was carried out at lab scale in order to assess the capability of the developed flexible coating to preserve the efficiency of solar cells

In particular, this final phase of the study was aimed to compare the stability obtainable by flexible coatings with the glass and to investigate the effect of the novel passive multi-barrier coating previously developed in comparison with the standard flexible materials. This research activity is still in progress and at date only preliminary data were obtained.

Another approach that was followed during the PhD study was aimed to develop an active barrier coating for solar cells able to continuously adapt its protective action according to the intensity of the environmental degradation phenomena. The driving idea is that of including in suitable and transparent polymer substrate specific oxygen absorbers, which are activated by meteorological phenomena (diurnal temperature variation, rain, etc.). This system may offer an active and dynamic protection able to react to the environmental changes. There are only few theoretical studies considering the use of suitable oxygen scavengers to be included in polymer barrier layers for solar cells, (Amberg-Schwab et al. 2006) essentially based on the use of oxygen scavenger systems activated by UV radiation.

Furthermore, there are some commercial products that were recently introduced by SAES Getters[6] with active barrier properties for water vapor. However, these products need to be stored in nitrogen atmosphere and at low temperature before they are applied and also have some drawbacks concerning the optical properties.

The research activity on the active barrier layers provided some preliminary but encouraging results that represent a basis for future study in this field.

The coating materials studied and developed with the above approaches are thought to be included in a multilayer structure where they can act synergically in order to guarantee a better protection to the flexible solar cell, like shown, for instance, in fig. II.2.

---

[6] www.saesgetters.com

Gas Passive barrier layer
Gas Active barrier layer
Liquid barrier layer
Solar cell
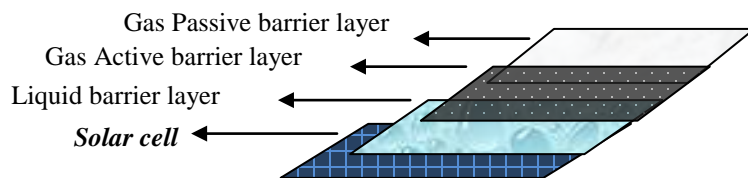
Figure II.2 *Schematic representation of a multilayer structure hypothesis*

The experimental work that was performed for pursuing the envisaged objectives of studying new flexible barrier materials to enhance the solar cells durability is reported in the following chapters. Four main phases may be identified in the research workflow:

- study and development of flexible multi-barrier coating materials, included in chapter III
- study and development of active barrier materials, reported in chapter IV
- development and characterization of multilayer coatings, described in chapter V
- encapsulation of organic solar cells with the developed materials in order to assess their effectiveness in improving the solar cells durability, also reported in chapter V.

Chapter III
Passive Multi-barrier layers

III.1 Introduction

This chapter includes the description of the study of a multi-barrier nanocoating, for enhancing the photovoltaic devices durability. In particular, the nanocoating integrates into a single layer more barrier functionalities: oxygen barrier properties, hydrophobic and oleophobic properties.

This nanocoating is deposited on standard solar cells coating organic-inorganic bilayers by applying the Self Assembly of Monolayers (SAM) technique, which represents a powerful and versatile strategy to create substrates with controlled molecular-level physicochemical characteristics (Lee et al. 2007).

Self assembled monolayers are ordered molecular assemblies that are formed spontaneously by the adsorption of a surfactant with a specific affinity of its endgroup to a substrate (Fig. III.1).

In particular a SAM structure of (fluoro)alkylsilanes chemisorbed on the inorganic layer of a inorganic-organic substrate (e.g. PET-SiOx) is expected to add hydrophobic and oleophobic functionalities to the film surface and also, hopefully, to increase the barrier properties of the substrate.

Considering that inorganic/organic bilayers such as PET-SiOx are the basic units which compose the multilayer barrier film used for protecting PV cells, a reduction of the number of bilayers that is necessary to ensure the solar cells durability may be achieved with this approach as a consequence of the improved barrier of the single bilayers.

As already discussed in Chapter II, the approach is novel in comparison with the related works, since it consists in the study of a single step room temperature process instead of multistep and complex processes. Furthermore, to our knowledge, both gas and liquid barrier properties of the modified surfaces were not investigated in the literature except for the study of Teshima at. al. However, the optical transparency properties were not analyzed in that study and the obtained performancesin terms of gas (O_2) and

liquid barrier improvement were too moderate to be considered of interest for PV applications (see tab. III.8 for a comparison analysis of the present approach and the related works).
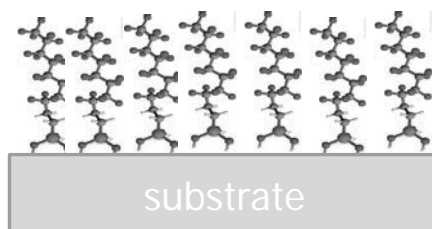
Figure III.1 *Schematic exemplification of a SAM*

III.2 Experimental Details

III.2.1 Materials

The following reagents were used: 1) octadecyltrimethoxysilane (OTS) provided by Aldrich and 2) 1H,1H,2H,2H-per-fluorodecyltrichlorosilane (FAS), provided by Alfa Aesar.

The (fluoro)alkylsilanes deposition experiments were carried out on two kind of flexible and transparent bilayer substrates: a) PETSiOx of 12 µm thickness provided by AMCOR[7] , composed of a polymer substrate (PET) with an inorganic coating (SiOx) layer of ~ 50 nm deposited with Electron Beam Evaporation, and b) ETFESiOx of 100 µm thickness provided by AMCOR , composed of a polymer substrate (ETFE) with an inorganic coating (SiOx) layer of ~ 50 nm deposited with Electron Beam Evaporation. Anhydrous toluene (distilled) and anhydrous ethanol ($H_2O \leq 0.01\%$), provided by Sigma Aldrich were used as solvent, alternatively.
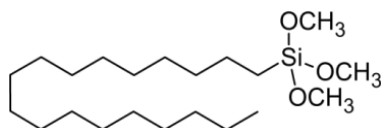
Figure III.2 *Chemical structure of the octadecyltrimethoxysilane (OTS).*
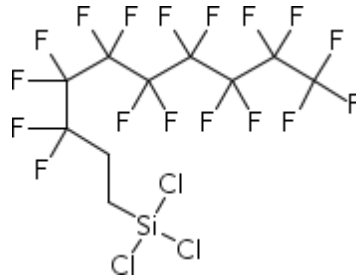
Figure III.3 *Chemical structure of the 1H,1H,2H,2H perfluorodecyltrichlorosilane (FAS).*

III.2.2 Deposition experiments for the preparation of nanocoated samples

The film samples of PET-SiOx and ETFE-SiOx were accurately cleaned before the deposition reaction, in order to remove all the impurities from the SiOx surface.

The cleaning procedure consisted of subsequent dipping cycles with toluene and distilled water with intermediate drying in N_2 flow. The deposition experiments were performed in a glass batch reactor where the substrate was placed.

The glassware was preliminary flame dried in order to remove any trace of water vapour and subsequently a N_2 atmosphere was maintained in the reactor.

The reactor was specifically designed during the PhD study in order to optimize the SAM deposition on these organic-inorganic substrate. The system was equipped with a sample holder in teflon allowing a quick and easy insertion/extraction procedure without any contact with the inorganic coating of the substrate sample, since its barrier properties are very sensitive to the mechanical abrasion effects (Fig. III.4).
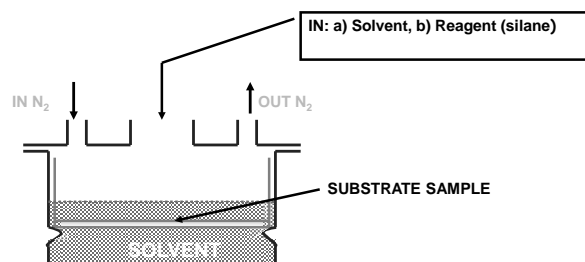
Figure III.4 *Schematic view of the reactor designed and used during the PhD study for the SAM deposition on the organic-inorganic substrates.*

For the reaction experiments two solvents were used, toluene and ethanol.

In a first experimental phase, silane deposition was performed by immersion of the substrate samples (surface area from 10 cm^2 to 80 cm^2) in 80 ml of a 1% (v:v) solution of silane (for both OTS and FAS experiments) in distilled toluene and under anhydrous conditions. Subsequently, different reagent v:v concentrations (1%, 3%, 5%), as well as a different solvent (ethanol), were used for the FAS deposition experiments.

The reaction was stopped after 12 hours and the obtained samples were then cleaned by subsequent dipping cycles with toluene and distilled water with intermediate drying in N_2 flow. PETSiOx substrates were also dipped for 12 hours in the solvents without reagents, in order to investigate eventual solvent induced modifications.

Codes of the produced samples: the produced samples will be indicated from now on in the text according to the following nomenclature: RZ-S, where: R is the reagent that can be OTS or FAS, Z is the v:v percent concentration of R in the solvent and S is the used solvent, that can be T (toluene) or E (ethanol). All the obtained samples are listed below according to the above defined nomenclature: OTS1-T, OTS1-E, FAS1-T, FAS3-T, FAS1-E, FAS3-E, FAS5-T, FAS5-E. The samples obtained by dipping the substrates in the solvents – toluene and ethanol - without reagents are indicated with PETSiOx-E and PETSiOx-T, respectively. The nanocoated sample of ETFESiOx is indicated as ETFESiOx FAS1-T.

III.2.3 Characterization of the nanocoated samples

FTIR (Fourier Transform Infrared Spectroscopy) measurements were carried out on the uncoated and coated samples in the range of 4000–650 cm using a Nexus ThermoNicolet spectrometer equipped with a SmartPerformer accessory for ATR analysis.

The hydrophobic properties of the obtained samples were assessed by means of static water contact angle measurements, performed by depositing 5 drops of distilled water of 2 μl on each side of the sample and then calculating the average values for each side.

Experimental measurements were performed with a First Ten Angstrom Analyzer System 32.0 (mod. FTA 1000) according to the standard test method ASTM D5946. The oleophobic properties were also preliminarily investigated by means of static oil contact angle measurements performed by depositing 3 drops of 2 μl of polyalphaolefinic synthetic oil PAO6 on each side of the sample and then calculating the average value for each side.

The OTR measurements were carried out with the Permeabilimeter GDP – C 165 provided by Brugger at 23°C and under oxygen flow of 80 ml/min, according to the standard ISO15165-1. Measurements at higher temperature (35 and 45°C) were also performed for studying a temperature range closer to the actual operating conditions of the PV devices.

The transparency was evaluated by measuring the UV-visible transmittance of the nanocoated surfaces from 200 nm to 800 nm with the UV-Visible Spectrophotomer λ 800 Perkin Elmer.

The surface morphology was characterized using a Nanoscope V multimode Atomic Force Microscope (Digital Instruments) and the root-mean-square roughness (Rq) values were calculated on scan areas of 5 μm x 5 μm with the Software Nanoscope Analysis of Bruker (version 1.40).

The thermal characterization was carried out with a Mettler Differential Scanning Calorimeter (DSC30), performing a dynamic 10°C/min rate heating scansion of the uncoated and nanocoated samples from -100°C to 300°C, followed by an isothermal scansion of 5 minutes at 300°C, by a subsequent cooling up to -100°C and then by a second heating up to 300°C (both at 10°C/min).

The heat of melting, ΔHm, and cold crystallization, ΔHc, were determined by integrating the areas (J/g) under the peaks.

The percent crystallinity values Xc were calculated according to the following equation:

$$\% \text{ Crystallinity} = [\Delta Hm - \Delta Hc]/\Delta Hm^0 * 100\% \qquad \text{(III.1)}$$

where ΔHm is the heat of melting, ΔHc the heat of cold crystallization and ΔHm^0 is the heat of melting if the polymer was 100% crystalline, taken

27

as reference value. The used reference heat of melting for PET-SiOx is the same value of PET (since the melting temperatures of SiOx are very high and are not reached during the DSC experiments) and is 140.1 J/g (W. J. Sichina).

III.2.4 Accelerate Ageing Tests

Usually, durability studies for coating materials of PV devices (but not specifically for this kind of hydrophobic coating materials) are conducted with damp heat and/or UV radiation exposure of the material samples (Jorgensen et al. 2006). Thus, an innovative element of this study consists in the methodology adopted for the accelerate ageing tests, which takes into consideration also the ageing degradation related to the acid and alkaline rains (J. Scheirs 2000).

The Ageing tests were designed and carried out in order to assess the aging effect on the coating materials barrier properties of the following atmospheric degradation agents: 1) acid and alkaline rains, 2) damp heat, 3) UV exposure.

III.2.4.1 Acid and alkaline rains.

Uncoated and coated samples have undergone a cyclic dipping treatment in water solutions at a pH varying during the time according to the scheme represented in figure below.

Table III.1 *pH variation in function of the accelerate ageing time.*

	1st cycle				2nd cycle							
pH	2	5,7	8	12	2	2	5,7	5,7	8	8	12	12
weeks	1st	2nd	3rd	4th	5th	6th	7th	8th	9th	10th	11th	12th

This method was designed in order to simulate the degradation effect of both acid and alkaline rains and the pH conditions selected for the ageing test are significantly more drastic compared to those of the natural phenomena. In fact, unpolluted rain has an acidic pH, but usually no lower than 5.7, because carbon dioxide and water in the air react together to form carbonic acid, while the presence of SOx and NOx in industrialized areas leads to the acidic rains (pH ≈4) phenomena (Reitze 2001). Furthermore, recent studies demonstrated that also alkaline rains may occur (pH≈ 8) (Ozsoy and Cemel Saydam 2000, Glaves et al. 2002, Avila et al. 1999).

28

Thus, the ageing cycles were thought and carried out in order to simulate the cyclic effect of alternating phenomena of acid, unpolluted and basic rains, and even more drastic pH conditions were created if compared with those of the natural acid and alkaline rains.

III.2.4.2 Damp heat accelerate ageing test

Uncoated and coated films have undergone ~ 700 hours test at temperature of 85°C and relative humidity of 85% according to the international standard test conditions IEC 61646:2008[8] in the climatic chamber CHALLENGE 250 (Angelantoni).

III.2.4.3 UV exposure accelerate ageing test

Uncoated and coated films have undergone ~ 700 hours test exposed at UV radiation at T= 60°C according to the international standard test conditions IEC 61646:2008.

III.3 Results and Discussion

III.3.1 Nanocoated PET-SiOx

In this work two molecules were tested for depositing the nanocoating on the silica surface of a PETSiOx substrate: a trimethoxysilne (octadecyltrimethoxysilane) and a trichlorosilane (1H,1H,2H,2H-per-fluorodecyltrichlorosilane).

The condensation reaction expected between the (fluoro)alkylsilane molecules and the silica surface of the PETSiOx substrate is shown in figure 2. The terminal groups, indicated with X in figure III.5, can be a chloride or a methoxy group, depending of the selected molecule for the deposition experiment.

All chlorosilanes react with water to produce hydrogen chloride and one or more of the silicon-chloride bonds becomes a silicon-OH bond. Similarly, methoxysilanes react with water to produce methanol and silanol groups (Si-OH) are formed. The hydroxylated silanes are highly reactive and will eventually bond to another OH on a solid oxide surface or react with another hydroxylated chlorosilane/methoxysilane. Water is a by-product of this reaction and a monolayer or also a multilayer of reticulated silanes may be generated (Fig. III.6).

---

[8] International Electrotechnical Commission Standard for Thin-film terrestrial photovoltaic (PV) modules - Design qualification and type approval
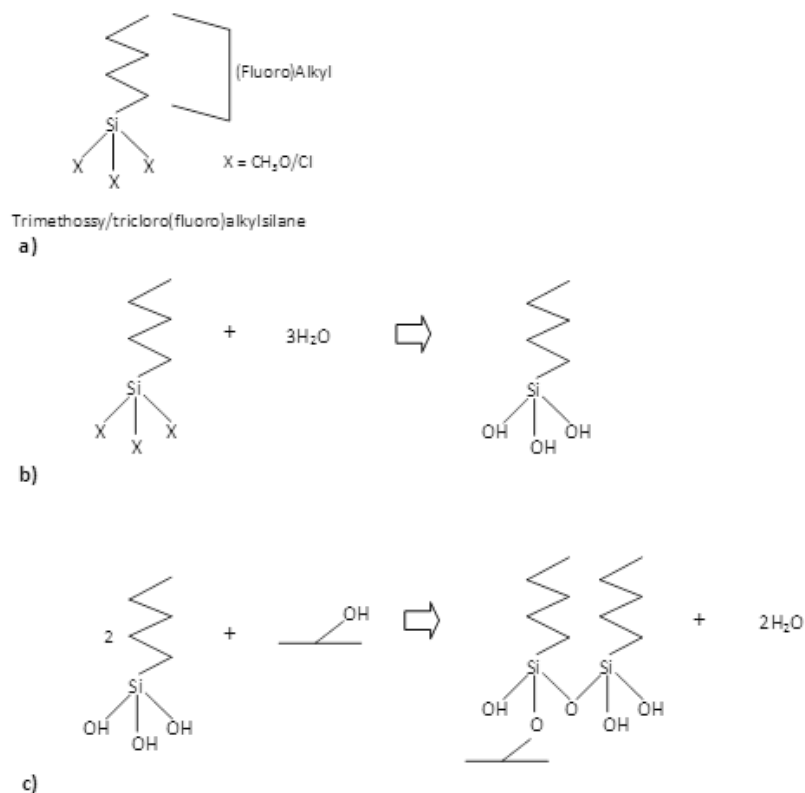
Figure III.5 *Illustration of silane chemistry a.) A schematic general representation of a trichlorosilane (or trimethoxysilane) b.) Hydrogen chloride (or methanol) is produced when chlorosilanes (or methoxysilanes) react with water resulting in a silicon-OH bond. c.) Highly reactive hydroxyl group bonds can react with a –OH on a solid oxide surface or another hydroxylated silane.*

30
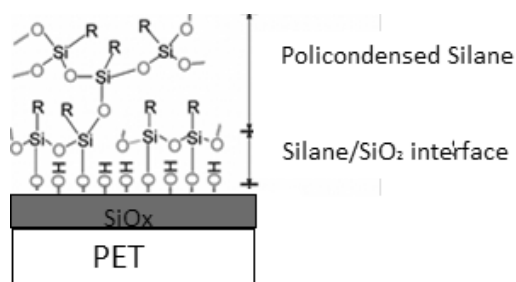
Figure III.6 *Schematic view of the policondensation product of silanes on a PET-SiOx substrate.*

III.3.1.1 ATR-FTIR Characterization

In order to verify that the condensation reactions of OTS and FAS on the PET-SiOx substrate successfully occurred, ATR-FTIR measurements were carried out on both the uncoated and the coated PET-SiOx samples and the obtained spectra are reported in figure III.7.

All the coated samples display similar bonding structures, independently from the silane nature and concentration used in the functionalization experiments, in the whole spectral region investigated. However, compared to the pristine PET-SiOx, and to the PET-SiOx dipped in the solvent without reagent the coated substrates show a change in the spectrum in the wavenumber range of $1300 \sim 1100$ cm^{-1}.

Despite the complexity of this region, where modes of Si-O bonds from silica and silane/silica interface overlap, in the spectra of the coated samples it can be clearly observed a new feature, appearing as a shoulder (just a little evident for the OTS 1-T sample) at about 1220 cm^{-1} of the broad Si-O band (1200-1300 cm^{-1}), which is assigned to Si-C linkages appeared after the condensation reaction (Oh and Choi 2010).

Correspondingly, the Si- OH bands in the range $3600 \sim 3100$ cm^{-1} of the coated samples almost disappear, confirming that the Si-OH groups on the silica surface reacted with the FAS and OTS silanes.

31
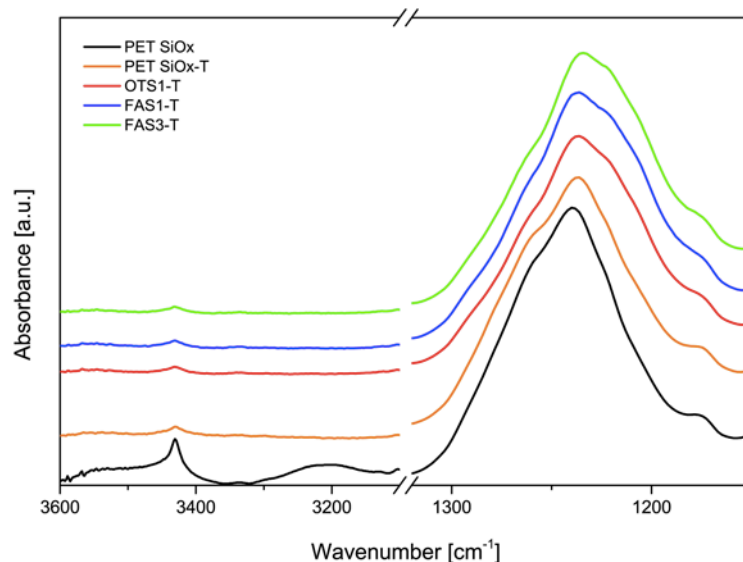
Figure III.7 *ATR-FTIR spectra of PET-SiOx (uncoated and only dipped in toluene without reagent), OTS coated and FAS coated samples.*

III.3.1.2 Liquid barrier properties characterization

The liquid barrier properties - hydrophobic and oleophobic - of the samples obtained depositing SAM nanocoating of OTS and FAS on the PET-SiOx substrates were assessed by static contact angle (CA) measurements and compared with those of the PET-SiOx samples, both uncoated and dipped in the solvent without reagents.

Figure III.8 shows the CA measurements for PET-SiOx, OTS1-T and FAS3-T samples.

In table III.2 the average water and oil CA values measured on the SiOx side are reported for the uncoated, OTS and FAS coated samples in toluene (1%, 3% and 5% v:v) and for the samples dipped in toluene without reagent, together with the calculated percent variation.

32

Table III.2 *CA average values on SiOx and PET sides, for uncoated, OTS coated and FAS coated samples (toluene)*

Sample	Static Contact Angle (CA) measurements (SiOx)			
	Water		Oil	
	CA average value [°]	% Δ after coating	CA average value [°]	% Δ after coating
PETSiOx	63 ± 5	-	43 ± 0.14	-
PETSiOx-T	58 ± 3	- 8	40 ± 5	-7
OTS1-T	86 ± 5	+ 37	37 ± 4	- 14
FAS1-T	112 ± 5	+ 78	70 ± 4	+ 63
FAS3-T	131 ± 2	+ 108	89 ± 4	+ 107
FAS5-T	112 ± 3	78	n.d.	n.d.

n.d. = not determined

The obtained data show that the chemical deposition of the OTS nanocoating causes an increase of 37% of the average water CA on the SiOx surface, while the FAS reagent is more effective since its nano-coating successfully changed the SiOx surface from hydrophilic to hydrophobic with a 78% increase of the average CA with respect to the uncoated PET-SiOx surface.

The treatment of the PET-SiOx samples with solvent without reagents does not modify the surface water wettability, since the variation of 5° in the average CA is negligible (Altavilla and Ciliberto 2011).

According to these results, further deposition experiments were carried out with FAS in order to study the effect of the reagent concentration.

As shown in tab. III.2, the best results were found for a 3% v:v concentration with average static CA higher than 130° as a consequence of the FAS deposition and a significant increase of 108% of the CA on the SiOx side.
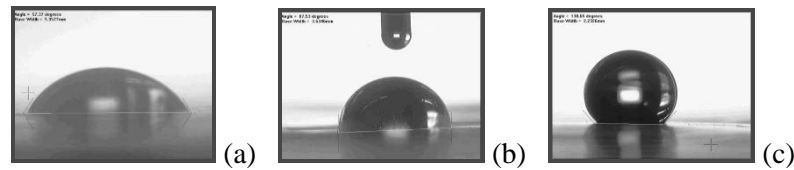
Figure III.8 *Pictures of water CA measurements on uncoated PET-SiOx (a), OTS1-T (b) and FAS1-T (c) samples.*

Concerning the oleophobic properties, OTS and FAS produce opposite effects on the coated surface. In fact, it is found (tab. III.2) that the OTS nano-coating reduces the oil CA average value (37°) as compared to that of uncoated PET-SiOx (43 °). This is clearly a consequence of the deposited OTS SAM, that promotes the oil wettability of the SiOx side due to the Van der Waals interaction of alkyl chains with hydrocarbons (McNaught et al. 2006).

On the contrary, the FAS nano-coating significantly improves the oleophobic properties (CA: 70° for FAS1-T sample) and the 3% FAS nanocoating (FAS3-T sample), in particular, almost doubles the oil CA value of the PET-SiOx substrate changing its surface from oleophilic to almost oleophobic (CA ~ 90 °). These preliminary results will support further research activity in order to improve the oleophobic properties, that are very interesting not only for the solar cells coating materials but also for other applications (e.g. touch-screen displays, etc.).

Water contact angle measurements were also performed on the PET side of the PET-SiOx substrate before and after nanocoating with OTS and FAS (at different concentrations). The resulting data are shown in figure III.9 where the water CA average values on the PET side are compared with the obtained data on the SiOx side.

It may be observed that the FAS deposition modifies both the PET and SiOx surfaces while the same measurements carried out for the OTS coated samples suggest that only the SiOx surface was coated, since the 7% increase found for the PET side is negligible (Altavilla and Ciliberto 2011).
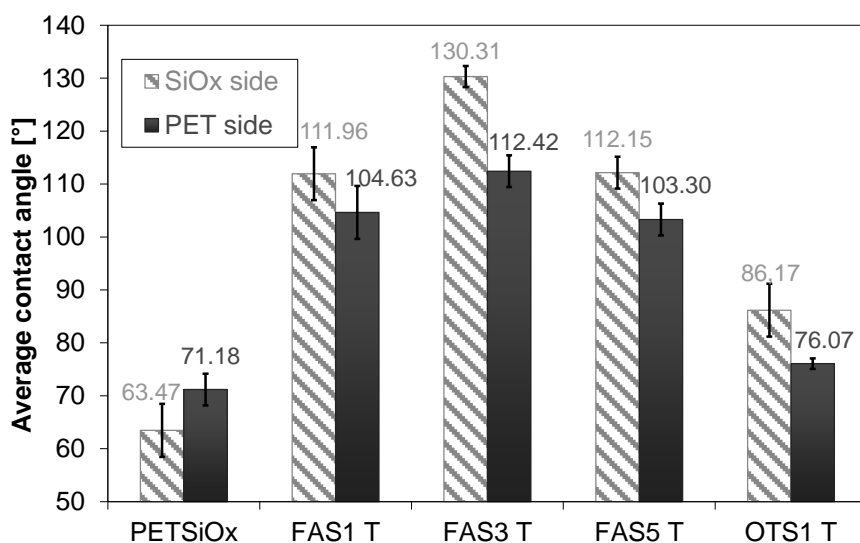
Figure III.9 *Effect of the reagent typology (FAS/OTS) and of the reagent (FAS) concentration in toluene on the average contact angle measured on PET and on SiOx surfaces before and after the deposition.*

III.3.1.3 Chemical Mechanism Hypothesis

A chemical mechanism is proposed in order to explain the different reactive behaviour of the PET-SiOx samples with FAS and OTS, respectively.

The OTS reaction (Fig. III.10) with SiOH sites foresees 2 steps (Brinker 1988), the first one between the H_2O molecules and the alkoxy groups (CH_3O-) and the second one between the OTS-SiOH and the hydroxyl groups on the silica surface.

The reaction mechanism for the FAS condensation (Fig. III.11) is very similar to that of OTS, the only difference consisting in the formation of hydrochloric acid, instead of methanol, as intermediate product. The presence of HCl leads to the activation of reactive hydroxyl groups also on the PET surface of the substrate (Ravens 1960) and this is the suggested explanation for the double-side modification deduced from the CA measures performed on the FAS coated samples.

1. OTS hydrolisys

2. OTS condensation on SiOx side

Only the SiOx side is functionalized by OTS
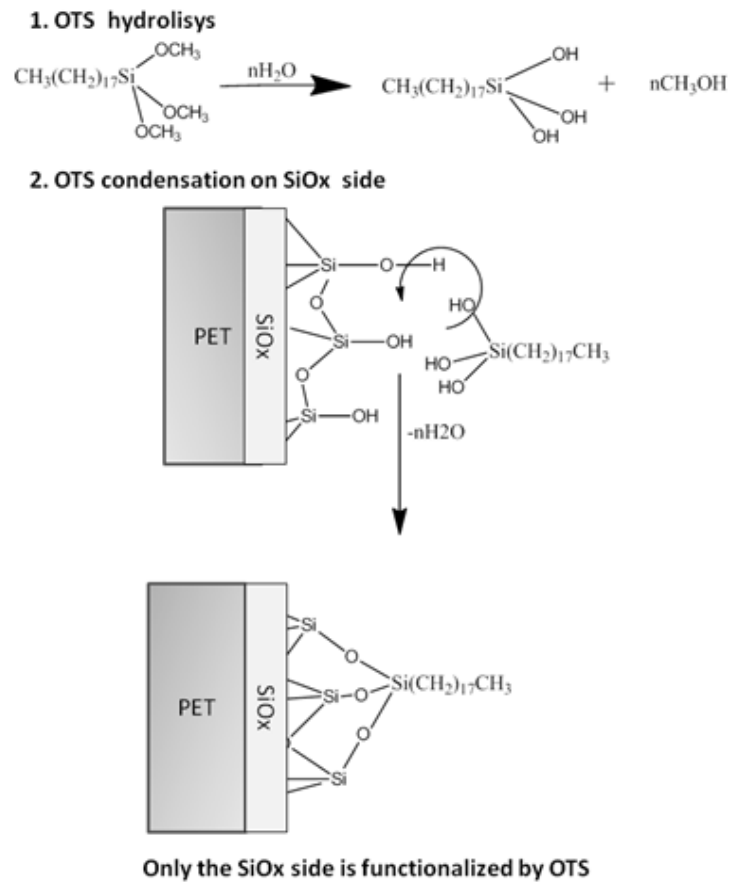
Figure III.10 *Hypothesis of reaction scheme for the OTS condensation.*

1. FAS hydrolisys

2. H₃O⁺ catalyzed hydrolysis of uncoated PET surface

PET

3. FAS condensation on hydrolyzed PET surface

4. FAS condensation on SiOx surface

Both sides are functionalized by FAS
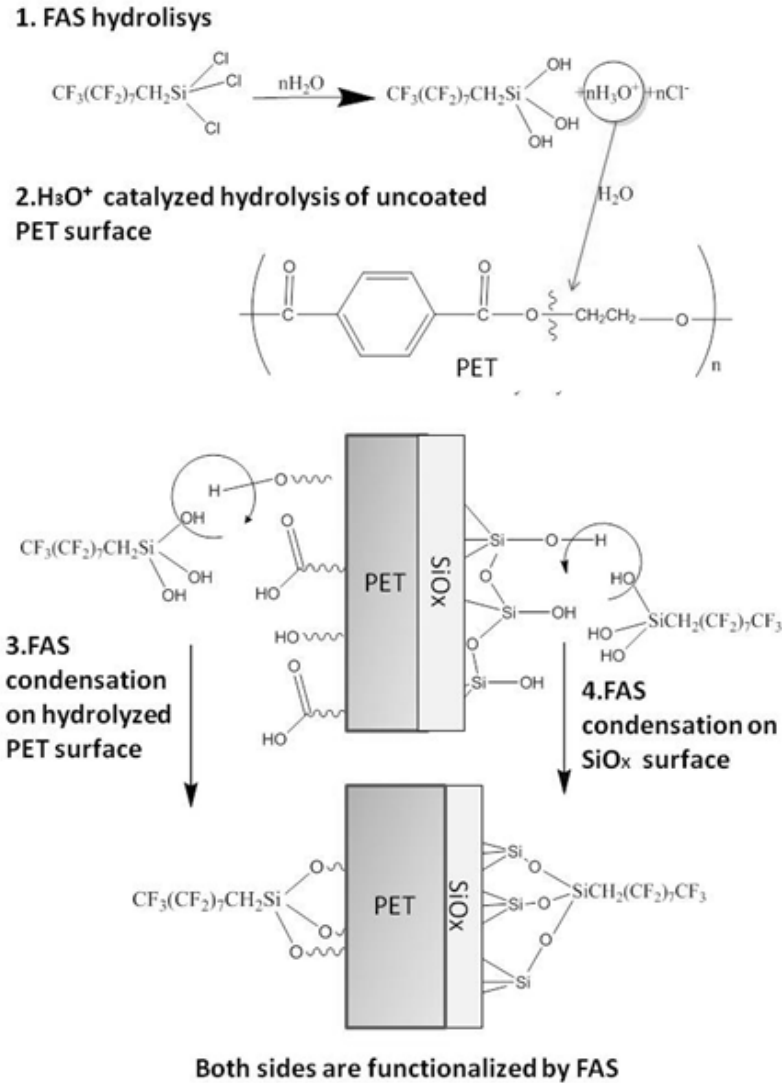
Figure III.11 *Hypothesis of reaction scheme for the FAS condensation.*

III.3.1.4 Optical Properties Characterization

Transparency properties are also very important for the front side coating materials of solar cells. The percent transmittance (%T) of the PET-SiOx samples coated in toluene with OTS and FAS was measured in the UV-

37

visible range and compared to that of the uncoated PET-SiOx and of the PETSiOx substrate dipped in the solvent (toluene/ethanol) without reagents.

As illustrated in fig. III.12, the OTS coating does not affect the transparency of the PET-SiOx substrate, whereas the FAS coating is associated with some transparency reduction in the lower wavelength range. Identical trends were found for 1% and 3% FAS nanocoated samples in toluene. The dipping of PET-SiOx substrates in the solvents without reagents does not substantially modify the optical properties in our experimental conditions.
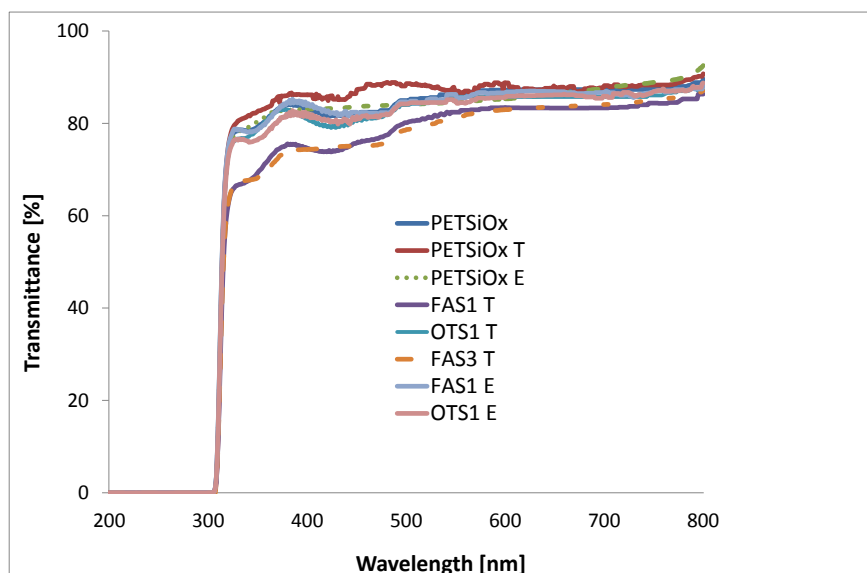
Figure III.12 *Effect of solvent (Ethanol/Toluene), of precursor molecule typology (OTS/FAS) and of its related concentration on the %transmittance in the UV-Visible range of PET-SiOx uncoated and coated samples.*

III.3.1.5 Surface morphology characterization

Furthermore, the surface morphology of the nanocoated samples was also analysed by Atomic Force Microscopy (AFM).

The arithmetic mean roughness (Ra) and the root-mean-square roughness (Rq) were calculated for the uncoated, OTS and FAS coated samples and are reported in Tab. III.3. It was found that OTS causes a small roughness increase if compared with the uncoated sample, while higher roughness is observed for the FAS coated surfaces (Fig. III.13).
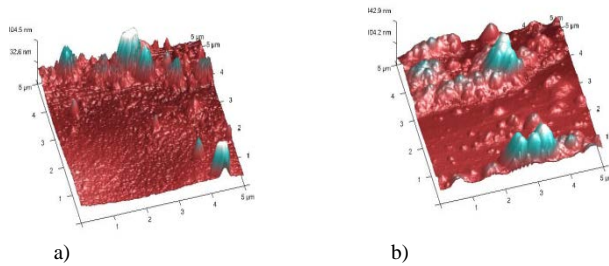
Figure III. 13 *AFM images with scan area 5 μm x 5 μm of a) PET-SiOx and b) FAS1-T samples*

Table III.3 *Arithmetic average roughness (Ra) and root-mean square roughness (Rq) for uncoated, OTS (1%) coated and FAS (1%) coated samples of PETSiOx. Scan area 5 μm x 5 μm.*

Sample	Ra [nm]	Rq [nm]
PET-SiOx	11	19
OTS1-T	18	25
FAS1-T	53	73

Transparency and roughness are competitive properties, and this is confirmed by the comparison of characterization data of transparency and surface morphology, respectively. In fact, the higher Rq value of the FAS coated sample corresponds to a small drawback in terms of transparency reduction.

Clearly, the transparency reduction is a consequence of the scattering effect (Gouesbet and Gréhan 2011), occurring when the wavelength of the

incident light becomes comparable with the protrusions dimension, found in the order of ~ 400 nm for the FAS coated samples.

Better transparency results were found for the FAS coated samples obtained using ethanol instead of toluene as solvent in the deposition experiments, as shown in fig. III.12.

III.3.1.6 Effect of solvent on the hydrophobic properties

The results of water CA measurements performed on coated samples using ethanol as solvent are shown in tab. III.4, and a comparison of the obtained data with toluene and ethanol is shown in fig. III.14. From table III.4 it may be noticed that the dipping of samples in ethanol without reagents does not influence the water wettability of the surface.

Table III.4 *CA average values on SiOx and PET sides, for uncoated, OTS coated and FAS coated samples in ethanol*

Sample	Static Water Contact Angle (CA) measurements			
	SiOx Side		PET side	
	CA average value [°]	% Δ after coating	CA average value [°]	% Δ after coating
PETSiOx	63 ± 5	-	71 ± 3	-
PETSiOx-E	62 ± 5	− 2	74 ± 9	+ 4
OTS1-E	89 ± 4	+ 29	72 ± 1	+ 1
FAS1-E	104 ± 5	+ 65	101 ± 3	+ 42

It can be seen from figure III.10 that the experimental results of OTS deposition are not substantially affected by the solvent change, while the FAS deposition experiments produce slightly better results when performed in toluene. This is probably due to the reduced H_2O content of the distilled toluene (totally anhydrous) if compared to the used ethanol ($H_2O \leq 0.01\%$). In fact, the small H_2O traces present in the ethanol solvent are likely to reduce the effectiveness of the FAS deposition, rather than that of the OTS one, because of the FAS higher reaction kinetics due to the chloride functional groups. Thus, in the presence of small traces of H_2O in the bulk of the ethanol solvent, a competing mechanism of polymerization of the FAS molecules may start before the molecules reach the PET-SiOx substrate,

leading to a reduced reaction efficiency for the SAM deposition on the substrate.
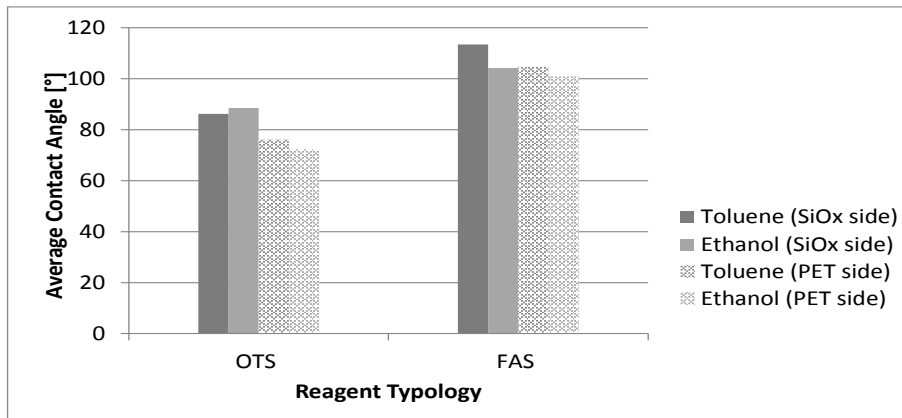
Figure III.14 *Effect of the solvent (toluene/ethanol) selection on the average contact angle after deposition with OTS and FAS (1%v:v).*

III.3.1.7 Oxygen Barrier Properties and thermal characterization

The oxygen barrier properties of the hydrophobic nanocoating were also investigated and OTR measurements were performed at three different temperatures: 23°C, 35 °C and 45°C for coated and uncoated samples since the barrier properties at higher temperatures are particularly interesting for PV applications. The best and more representative samples were selected for the gas barrier analysis: the FAS3-T (best hydrophobic properties), FAS1-E (good hydrophobic properties and best transparency) and OTS1-E and PETSiOx for comparison purposes.

As can be seen from table IV, samples OTS1-E and FAS3-T show some slight reduction of OTR only at higher temperatures, while significant improvements are found for sample FAS1-E, at all temperatures, with a reduction of the OTR value to less than 1/3 if compared to that of the uncoated PET-SiOx sample (see table III.5).

41

Table III.5 *OTR for uncoated and coated PET-SiOx samples (OTS 1% in ethanol, FAS 1% in ethanol, FAS 3% in toluene).*

T [°C]	OTR [cm^3/m^{2}day bar] for PETSiOx (12 µm thickness) uncoated and coated with SAM			
	PET-SiOx	OTS1-E	FAS1-E	FAS3-T
23	11.4	12.2	3.8	11.4
35	21.5	18.3	5.9	16.7
45	31.0	27.2	9.1	23.8

For a passive barrier material, OTR is related to permeability (P) by the thickness (d) of the layer:

$$OTR = P/d \qquad (III.2)$$

Figure III.15 shows the oxygen permeability trend as a function of temperature for uncoated and coated films. It may be seen that all the coated films cause a stabilizing effect by improving the barrier properties of uncoated films at higher temperatures, which are typically reached during the normal operational lifetime of PV devices. As already said before, the best performance in terms of oxygen barrier properties are exhibited by the FAS coating carried out in ethanol.

Permeability often follows an Arrhenius dependence on temperature (T):

$$P = P_0 e^{-E_p/kT} \qquad (III.3)$$

where Ep is the activation energy for permeation and k is the Boltzmann constant ($8,61*10^{-5}$ eV/K).

The activation energy values were calculated for uncoated and coated samples and are reported in Tab. III.6. It may be observed that all the coated films show a slight reduction of Ep in comparison to the uncoated PET-SiOx films.

Table III.6 *Activation Energy for uncoated and coated samples.*

Energy for uncoated and coated samples.

Sample	Ep [eV]
PET-SiOx	0.371
FAS3-T	0.269
OTS1-E	0.294
FAS1-E	0.322

Furthermore, a thermal characterization performed on the above samples showed negligible increase of the percent crystallinity X_c values after the FAS/OTS coating (tab. III.7). Therefore, the gas barrier improvement found for the FAS coating in ethanol is not related to a crystallinity increase, but can be the result of the competing polymerization mechanism of the FAS molecules occurring in the ethanol solvent, leading to the formation of a dense and more reticulated hydrophobic layer deposited on the PET-SiOx substrate.

Table III.7 *Percent crystallinity for uncoated and coated samples*

Sample	Xc
PET-SiOx	31%
FAS3-T	35%
OTS1-E	33%
FAS1-E	33%
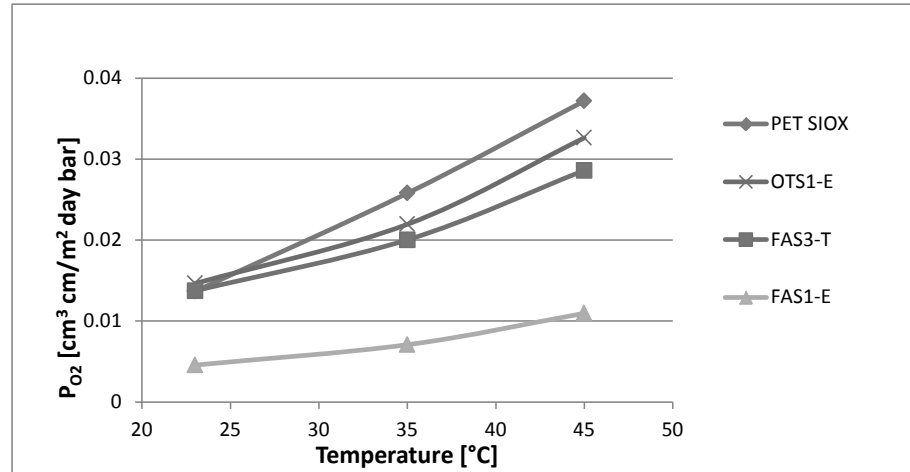
Figure III.15 *Oxygen Permeability in function of temperature for uncoated and coated PET-SiOx samples*

III.3.1.8 Synoptic Analysis of data

Fig. III.16 shows a comparison of the optical and barrier properties – liquid and gas – for the uncoated PET-SiOx and the most representative coated samples.

Transparency values are percent normalized assuming a 100% value for the uncoated sample. The liquid barrier properties are percent normalized values calculated assuming a 100% value for a water contact angle of 180°. The gas barrier improvement is calculated as the percent OTR reduction of the coated samples compared to the uncoated one.

It can be seen that the sample FAS3-T has the higher liquid barrier properties while the sample FAS1-E is the best in terms of gas barrier improvement. The coated samples leave substantially unmodified the transparency of the uncoated PET-SiOx, except of the FAS3-T which leads to a small reduction of transparency.

44
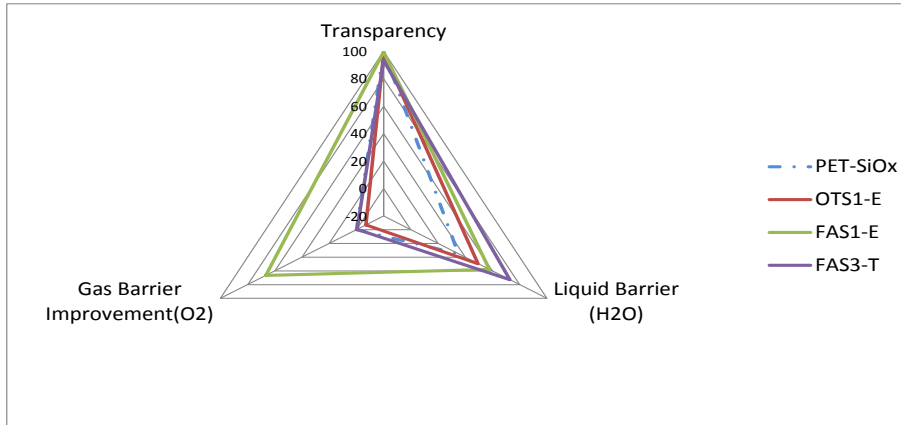
Figure III.16 *Radar chart of samples: PET-SiOx, OTS1-E, FAS1-E, FAS3-T: transparency-oxygen barrier-water barrier.*

Table III.8 summarizes a comparison of the performances obtained with our approach with those reported in the related works (Karunakaran et al. 2011, Lu et al. 2011, Xiu, et al. 2008, Ling et al. 2009 and Teshima et al. 2003).

It may be seen that our approach allows to obtain - with a single step and at room temperature process- hydrophobic properties that are only 13% lower if compared to those obtained with multistep and high temperature processes (Xiu et al. 2008, Ling, et al. 2009), while the hydrophobicity is 30% higher of that reported by Teshima et al. (2003) on similar substrates.

The oxygen barrier properties are also significantly better for the present study if compared to those obtained by Teshima et al. (2003).

Table III.8 *Comparison analysis of obtained results: Present Study vs Related Works*

	Related Works				Present Study
	[K]	[X]	[L]	[T]	
Process characteristics	Multistep with O_2 plasma treatment and T= 160°C[a] step	Multistep with electron beam evaporation and T= 85°C step	Multistep process with T= 1100°C step	Multistep with T= 100°C step	Single Step, Room Temperature
Substrate typology	Si, glass, polyester	Si	Glass/Silicon Oxide	PET-SiOx	PET-SiOx
Obtained Properties					
Water CA [°]	>160	>150	>150	>100	>130
Oil CA [°]	>110	n.i. [b]	n.i.	n.i.	~90
OTR reduction [%]	n.i.	n.i.	n.i.	~ 40%	67%
Optical transparency	Similar to uncoated sample	n.i.	Similar to uncoated sample but some scattering at λ < 500 nm	n. i.	Similar to uncoated sample

K: Karunakaran et al. 2011, X: Xiu et al. 2008, L: Ling, et al. 2009, T: Teshima, et al. 2003)
[a] for polyester substrate
[b] n.i. = not investigated

III.3.2 Nanocoated ETFESiOx

The SAM deposition was preliminarily studied also on another organic-inorganic substrate, ETFE-SiOx, which is applied as flexible frontsheet for solar cells protection for its weather resistance characteristics. The reaction experiments were carried out in toluene and with 1% concentration of FAS reagent (see section III.2.2).

III.3.2.1 Hydrophobic properties characterization

The CA measurements carried out on uncoated and FAS nanocoated ETFE-SiOx showed that a significant increase of 397% of the average CA was obtained with the FAS SAM (tab. III.9), which changed the SiOx surface from hydrophilic to hydrophobic (Fig. III.17).

Table III.9 *CA average values for uncoated and coated ETFESiOx (for both sides)*

Sample	Static Water Contact Angle (CA) measurements			
	ETFE side		SiOx side	
	CA average value [°]	% Δ after coating	CA average value [°]	% Δ after coating
ETFE-SiOx	91.63 ± 6	-	21.7 ± 5	-
ETFE-SiOx FAS1T	83.49 ± 15.2	-8	107.9 ± 10	+ 397
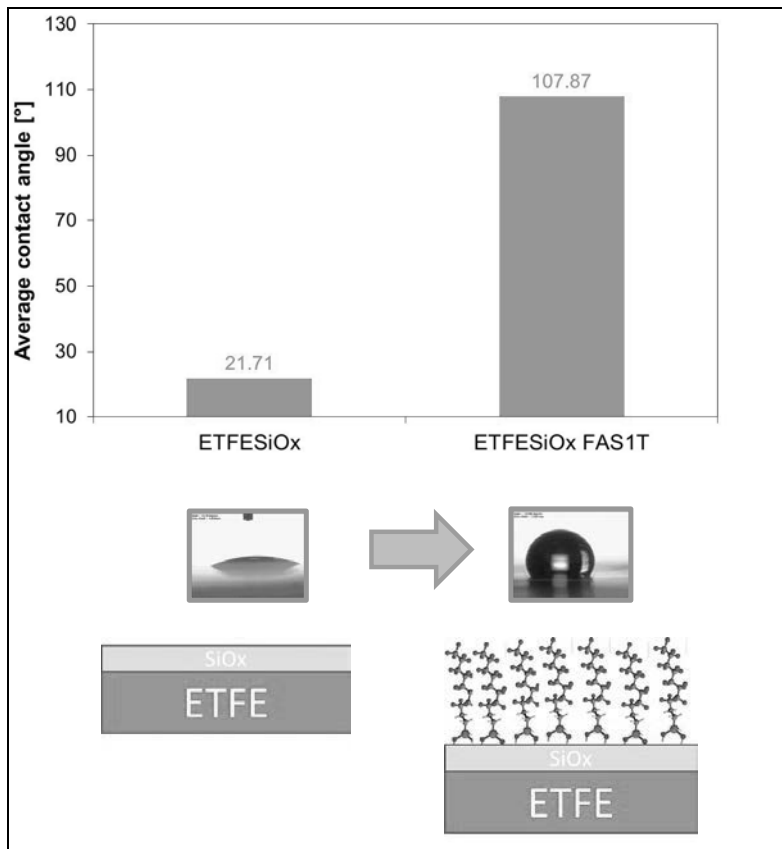
Figure III.17 *Static water CA for ETFESiOx uncoated and coated with FAS SAM (average values calculated on the SiOx surface).*

47

III.3.2.2 Optical Properties Characterization

The percent transmittance of coated and uncoated ETFE-SiOx was assessed in the UV-Visible range. As can be seen in Fig. III.18, in this case the transparency was not substantially affected by the FAS nanocoating, since the reduction of %T may be considered negligible.
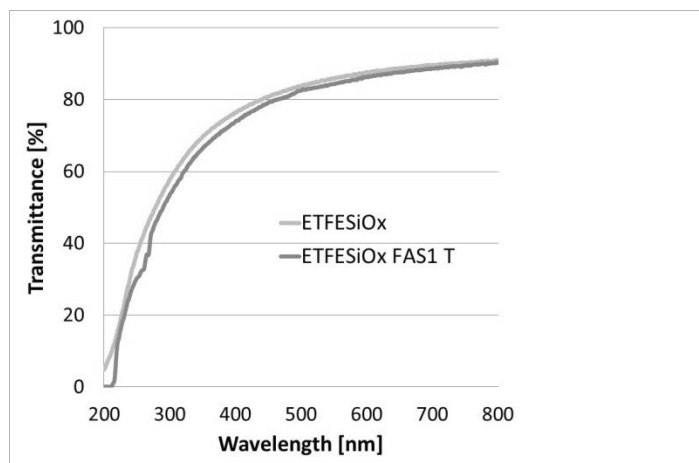
Figure III.18 *% Transmittance in the UV-visible range for ETFE-SiOx uncoated and coated with FAS (1% v:v in toluene).*

Thus, after the SAM noanocoating the ETFESiOx layer may continue to act as an effective frontsheet for its transparency (about 90% at the plateau) but presents the additional advantage of the hydrophobic properties for a better protection of the coated solar cell.

III.3.2.3 Oxygen barrier properties characterization

The Oxygen barrier properties were evaluated for both the nanocoated and uncoated samples and the obtained results in terms of oxygen transmission rate and permeability are reported in tab. III.10 and in tab. III.11, respectively.

The obtained results showed that that no oxygen barrier improvements were achieved with the FAS nanocoating on the ETFESiOx, with the OTR value remaining approximately the same of that of the uncoated substrate at 23°C. A slight reduction of the oxygen barrier properties was observed at higher temperatures, that could be linked to an interaction of the toluene with the organic substrate.

These aspects will be further investigated with a thermal characterization as well as by performing tests on ETFESiOx samples dipped in the solvent

without the reagent, as performed for the PETSiOx samples (see section III.3.1).

Thus, only the improvement of the liquid barrier properties is achieved for the ETFESiOx substrate with the FAS SAM, while for the PETSiOx substrate also a significant oxygen barrier improvement was obtained (see section III.3.1.7).

However, the completion of these preliminary data with the results of further analysis of samples obtained with deposition experiments in ethanol will probably add more interesting information.

Table III.10 *OTR for ETFE, ETFE-SiOx samples coated and uncoated (FAS 1% v:v in toluene).*

T [°C]	OTR [cm^3/m^{2}day bar] for ETFESiOx (100 µm thickness) uncoated and coated with FAS SAM	
	ETFESiOx	ETFESiox FAS1T
23	63	79
35	90	115
45	134	201

Table III.11 *Permeability for ETFE-SiOx samples coated and uncoated (FAS 1% v:v in toluene).*

T [°C]	P [cm^{3}cm/m^{2}day bar] for ETFESiOx (100 µm thickness) uncoated and coated with FAS SAM	
	ETFESiOx	ETFESiOx FAS1T
23	0,6	0.79
35	0,9	1.15
45	1,34	2.01

III.3.3 Accelerate Ageing Tests

Accelerate Ageing Tests were performed on the nanocoated and uncoated samples in order to assess the resistance of the nanocoating to different environmental ageing factors (pH, temperature, RH, UV exposure).

To this aim, the obtained samples were subjected to drastic environmental conditions to simulate stressing ageing environmental phenomena such as acidic and basic rains, damp heat conditions, etc..

The hydrophobic properties of the aged samples were assessed during the ageing tests at regular time intervals.

III.3.3.1 Dipping in basic and acid solutions

Accelerate ageing tests were performed by submerging the nanocoated and uncoated samples in acidic and basic water solutions, alternatively, following 2 subsequent cycles as described in section III.2.4.1.

Figure III.19 shows the hydrophobic properties trend in function of the ageing time for the PET-SiOx uncoated and nanocoated substrate.
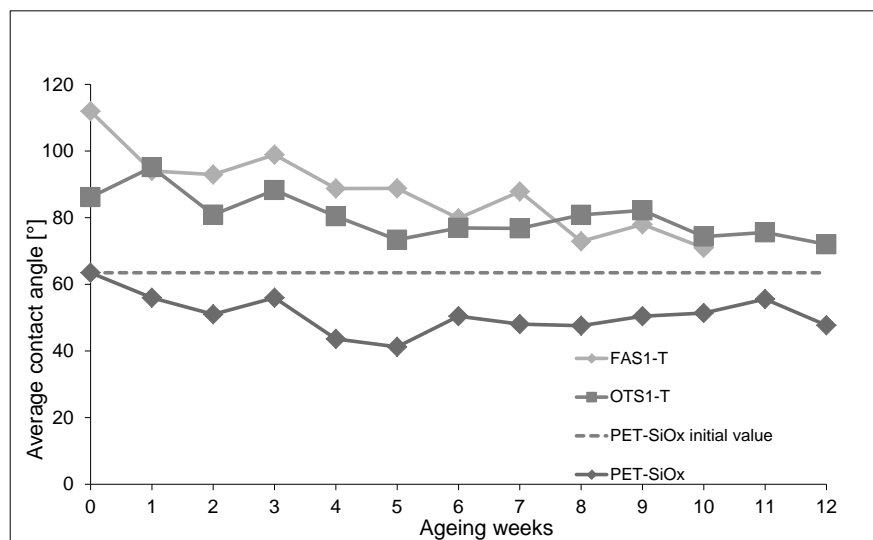
Figure III.19 *CA average values measured during the accelerate ageing test with cyclic dipping in varying pH solutions for uncoated, OTS coated and FAS coated PETSiOx samples.*

From Fig. III.19 a CA decreasing trend may be observed for all the aged systems.

In spite of the very drastic conditions (including different cycles at pH 2 and pH 12 that are not present in the "natural" acidic and basic rains) of this ageing test, the liquid barrier properties of the coated films show a good resistance exhibiting hydrophobic properties also after 7 weeks of treatment (more than 1100 hours of test duration). In particular, it is to be highlighted that the FAS nanocoated sample maintains a high hydrophobicity even after more than 1000 hours of accelerate ageing The tests were stopped once the CA values of the coated samples almost reach the initial value of the uncoated film, thus suggesting that the hydrophobic effect that had been added with the nanocoating was canceled.

50

In Fig. III.20 the hydrophobic properties in function of the ageing time are reported also for the ETFE-SiOx (uncoated and FAS coated). It can be seen from Fig. above that the average contact angle on the SiOx side of the uncoated ETFE-SiOx increases quite quickly during the first 4-5 weeks, and, subsequently, grows slowly reaching an asymptotic value very close to that of the ETFE side, suggesting that the hydrophilic silica layer was deteriorated by the ageing treatment. The hydrophobic coated substrate (ETFE SiOx FAS1T) follows a specular decreasing trend, quicker in the first 4-5 weeks and subsequently approaching an asymptotic value close to the average CA measured on the ETFE side, that is 91,63°(see Tab. III.9).

Figure III.21 shows the CA trend in function of the ageing time for both ETFE and SiOx sides of the uncoated substrate. It can be clearly observed that the of the ETFE side exhibits good resistance to the accelerate ageing while the SiOx side, on the contrary, undergoes a degradation phenomenon.

Furthermore, it is to be highlighted a higher stability of the coated ETFE-SiOx may be observed if compared to the uncoated sample, thus demonstrating a good resistance of the FAS nanocoating to such a drastic accelerate ageing condition.
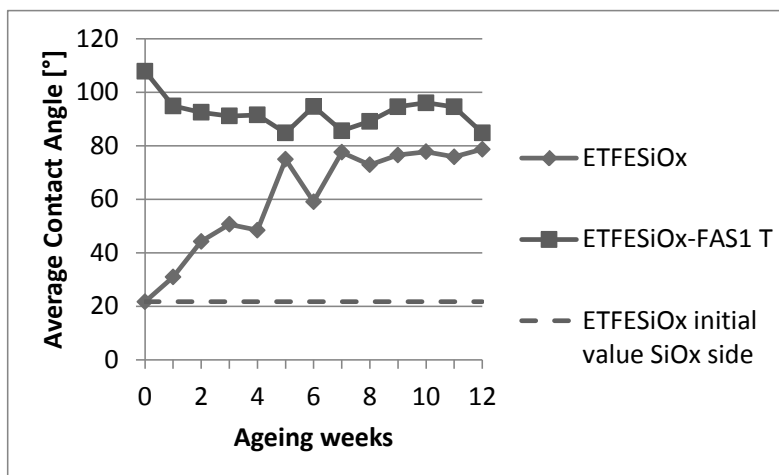
Figure III.20 *CA average values measured during the accelerate ageing test with cyclic dipping in varying pH solutions for uncoated, and FAS coated ETFE-SiOx samples.*

51
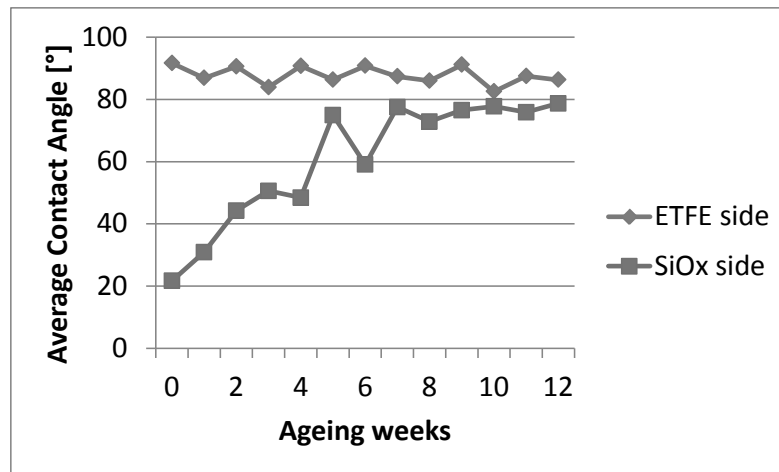
**Figure III.21** *CA average values measured during the accelerate ageing test with cyclic dipping in varying pH solutions for uncoated ETFE-SiOx on ETFE and SiOx sides.*

III.3.3.2 Damp Heat Accelerate Ageing

A damp heat accelerate ageing test of about 700 hours was carried for uncoated and nanocoated samples of both PET-SiOx and ETFE-SiOx samples at 85°C and R.H. of 85% according to the standard IEC 61646:2008.

In Fig. III.22 the hydrophobic properties in function of the ageing time are reported for the uncoated and nanocoated PET-SiOx samples.

It can be observed that the Damp Heat Ageing Test causes a small reduction of 5,65% (see Tab. III.12) of the hydrophobic properties for the FAS coated sample. The OTS coated sample seems to be not affected by the ageing test.

Furthermore, it can be noticed that the average CA on the SiOx side increases up to the value of the uncoated PET Side (see Fig. III.9).

Table III.12 *Average CA before and after the damp heat accelerate ageing test for samples PETSiOx, FAS 3T and OTS 1 E.*

	Average Contact Angle [°]		
Sample	**PETSiOx**	**FAS 3T**	**OTS 1E**
Before aging	63.47±5	102.68±2	88.50±4
After aging test	72.00±8	96.87±3	88,06±7
% change	*+13,44%*	*-5,65%*	*-0,5%*
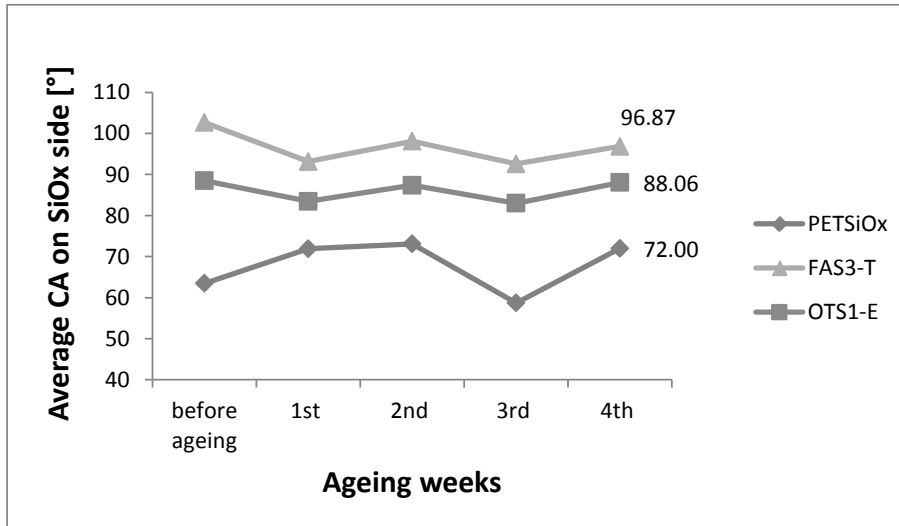
Figure III.22 *Average CA values in function of time during the damp heat accelerate ageing test on uncoated, FAS coated and OTS coated PETSiOx samples.*

In Fig. III.23 the trend of the hydrophobic properties in function of the accelerate ageing time is reported for the uncoated and FAS coated ETFE-SiOx samples.

A reduction of 10% of the hydrophobic properties was measured for the FAS coated sample which is still hydrophobic after 700 hours of accelerate ageing, thus demonstrating a good resistance of the FAS nanocoating.

It may be noticed in Fig. III.23 that the average CA on the SiOx side increases up to $\sim 80°$, that is very close to the average value of CA on the uncoated ETFE side. This suggests that a degradation of the SiOx layer occurred as a consequence of the accelerate ageing test for the uncoated substrate.

Therefore, the FAS nanocoating determines a higher stability of the substrate and supports the preservation in drastic accelerate ageing conditions of the SiOx layer. Consequently, the FAS nanocoating also helps to maintain the gas barrier properties of the substrate, that are essentially related to the inorganic layer.
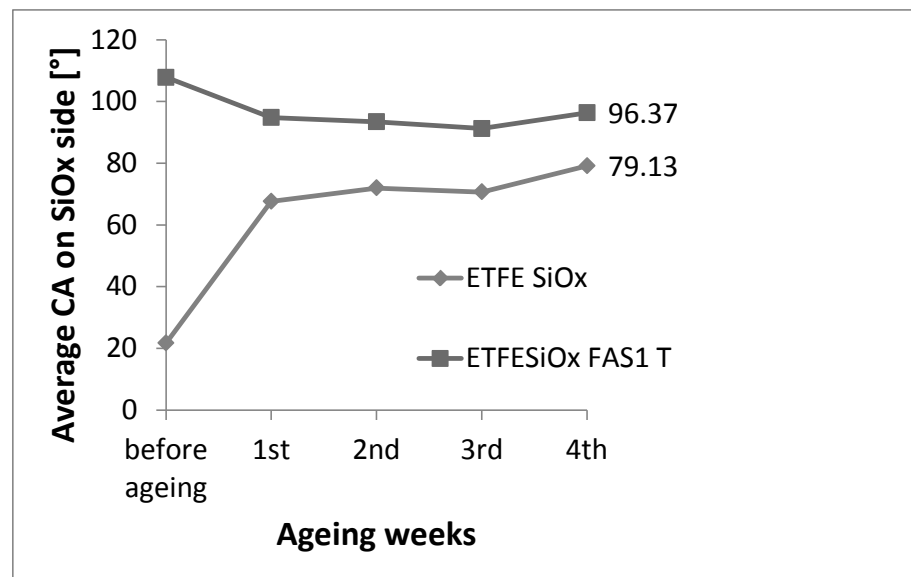
Figure III.23 *Average CA values in function of time during the damp heat accelerate ageing test on uncoated and FAS coated ETFE-SiOx samples.*

III.3.3.3 UV exposure accelerate ageing test

After the Damp Heat Ageing Test, the PETSiOx uncoated and coated samples underwent an UV exposure accelerate ageing test of ~ 700 hours. The hydrophobic properties trend in function of the ageing time is shown in Fig. III.24.
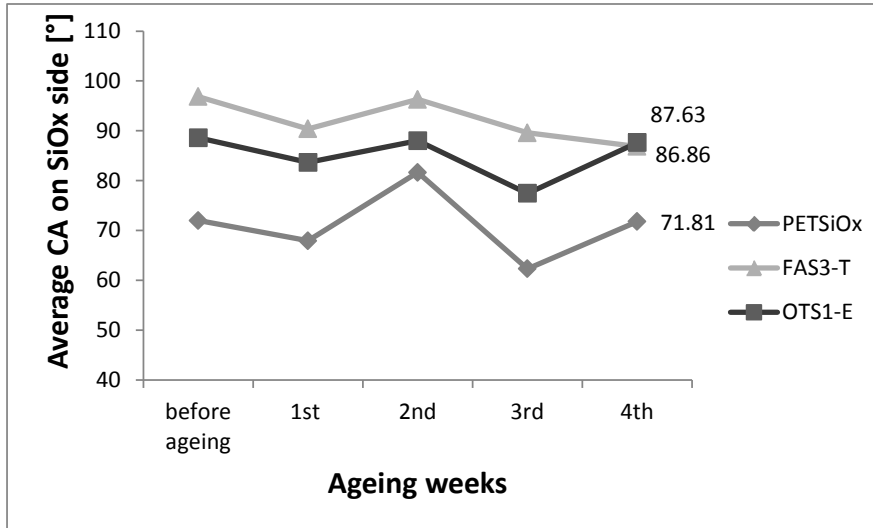
Figure III.24 - *Average CA values in function of time during the UV exposure Accelerate Aging Test on uncoated, FAS coated and OTS coated PETSiOx samples.*

From Fig. III.24 it can be seen that 700 hr of accelerate ageing with UV exposure at T = 60°C don't affect substantially liquid barrier properties of the nanocoated sample, since the FAS 3T sample still remains hydrophobic after the test completion.

III.3.4 Conclusions

The obtained results demonstrated that a high barrier flexible and transparent coating may be successfully obtained by modifying PV standard coating bilayers for solar cells such as PET-SiOx and ETFE-SiOx, with a simple and single-step process carried out at room temperature. The nanocoated films showed high hydrophobic properties and a significant improvement of the oxygen barrier properties, reducing the OTR to 1/3 of the corresponding value of the uncoated film.

Ageing tests were performed in order to verify the chemical resistance of the nanocoating material with accelerate ageing test simulating the degradation effect of both acidic and basic rains, damp heat, UV exposure.

The measured contact angle values showed that after an initial slight reduction of the contact angle value, a constant hydrophobic value was maintained for the FAS modified samples, even after the very drastic test conditions.

It is believed that an interesting contribution may be provided from the accomplishment of the present research activities to the PV sector

applications in terms of improved barrier properties of the coating materials for solar cells against liquid and gas atmospheric agents.

The so improved coating materials are expected to allow a reduction in the number of the necessary protective layers (see Chapter V), thus guaranteeing a higher lifetime for the PV modules at lower costs.

Chapter IV
Active Barrier Layers

IV.1 Introduction

In this chapter the results of the study of transparent and active barrier materials for flexible solar cells are reported.

As already discussed in the previous sections, solar cells require coating materials with high barrier properties in order to maintain a high efficiency during their lifetime, that are normally achieved using multilayer coatings (S. Logothetidis et al. 2010, Vaško et al. 2009, Visser 2008, Langereis et al. 2006, Rossi et al. 2014). However, these coatings basically consist of passive barrier materials, and thus they are not capable of modulating and adapting their response to the environmental change.

The protective action of the passive barrier materials can be significantly enhanced and strengthened by the addition of an active barrier coating (Rooney 1995, Galdi and Incarnato 2011), able to continuously adapt its protective action according to the intensity of the environmental degradation phenomena. The driving idea is that of including in suitable polymer substrate specific oxygen absorbers, which are activated by meteorological phenomena (diurnal temperature variation, rain, etc.). This system may offer an active and dynamic protection able to react to the environmental changes.

IV.2 Experimental details

Active Barrier films were produced by using pellets of PoliProtect APB (IV=0.85 dl/g, amount of oxidizable components 5.0 wt%) provided by M&G, a terephthalic acid (TPA)-based polyethylene terephthalate copolymer resin, with both active oxygen scavenger and passive barrier incorporated into the pellets. Each pellet, in fact, has a "passive barrier" inner layer, or core, made of Ultramid® X17 that is a partially aromatic copolyamide, and an outer layer made of a copolyester with cobalt salt. The cobalt in the outer layer catalyzes the "activation" of the inner core into an

"active" oxygen scavenging barrier (Fig. IV.1). The formulation contains also a ionic compatibilizer, consisting in a copolyester containing a metal sulfonate salt.
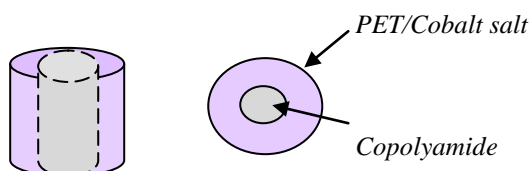
Figure IV.1 *Schematic representation of a Poliprotect APB pellet, with the internal phase of Ultramid® X17 copolyamide and the external phase of PET and a cobalt salt.*

In general, the oxygen scavenging is a complex and heterogeneous process, involving the physical dissolution into the polymer, oxygen diffusing through the polymer and reaction of the polymer with oxygen (Gillen et al 1992; Rincon-Rubio et al 2001).

The reaction mechanism is based on the oxidation of copolyamide that is catalyzed by cobalt salt (Bacskai et al. 1997): the oxidation of the copolyamide units under the condition of interest involved rather complex chemistry, and the details of the reaction are beyond the scope and the interests of the current study.

For comparison purposes, also the following standard PET matrix, without active phase, processable by film extrusion technology, were considered:

(a) Novapet MWsoft (I.V.[9] = 0.78 dl/g), provided by Novapet S.A.
(b) P60 (I.V. = 0.58 dl/g), provided by M&G.

IV.2.2 Processing

The films were manufactured using a laboratory-scale cast film extrusion line (THERMOPLASTICS Tokyo-Japan), equipped with a single screw extruder (screw geometry: D = 12, L/D = 24), a coat-hanger type head (slit die: 200 mm x 1 mm) and a take-up/cooling system (chill rolls). All the PETs pellets were preliminarily dried under vacuum for 14 h at 125°C before processing. In order to ensure the production of a stable and

---

[9] I.V.: Inherent Viscosity

continuous film without defects and of regular thickness, the processing parameters (melt and die temperatures, screw speed and cooling conditions) of the extrusion and the cooling stage of the film production were set on the basis of preliminary rheological and thermal analyses carried out on the pellets of the three PET samples.

The temperature profiles from the hopper to die were 300°C-290°C-290°C-280°C, for the Novapet and Poliprotect resin, and 285°C-280°C-280°C-275°C, for the P60 one. The screw speed was 50 rpm in all cases. The obtained film samples had thicknesses in the range 20-30 µm.

Fig. IV.2 *Extrusion of the Active PET Film with the lab-scale extruder (THERMOPLASTICS Tokyo-Japan).*

IV.2.3 Sample Characterization

Thermal characterization was carried out for pelletized and film samples of both active and reference PET with a Mettler Differential Scanning Calorimeter (DSC30), performing a dynamic 10°C/min rate heating scan of the polymer samples from -100°C to 300°C, followed by an isothermal scan of 5 minutes at 300°C, by a subsequent cooling scan up to -100°C and then by a second heating up to 300°C (both at 10°C/min). The heat of melting, ΔHm, and cold crystallization, ΔHcc, were determined by integrating the areas (J/g) under the peaks. The percent crystallinity values Xc were calculated according to the following equation:

% Crystallinity=$[\Delta Hm - \Delta Hc] / \Delta Hm^{0} \cdot 100$ (IV.1)

where ΔHm^{0} is the heat of melting (135 J/g) of ideal perfect PET crystals, taken as reference value (Knock et al. 1996).

59

The optical properties were evaluated by measuring the UV-visible transmittance of the obtained films from 200 nm to 800 nm with the UV-Visible Spectrophotomer λ 800 (Perkin Elmer).

Oxygen absorption measurements were performed with a Minisensor Oxygen Fibox 3-Trace v3 (Presens GmbH) by placing the active film of surface approx. 35 cm^2 in a vial of 9 ml volume. Oxygen absorption properties of the active films were studied in the following test conditions:

Table IV.1 *Humidity and temperature conditions used for the oxygen absorption measurements.*

Film Humidity Conditions	Short Denomination	T [°C]
Film conditioned at indoor relative humidity	Dry surface	25
Film with wet surface	Wet surface	25 – 45
Film immerged in water	In H$_2$O	25-35 – 45

The results are expressed as mg/l of oxygen in the test vial.

OTR measurements were carried out with the Permeabilimeter GDP – C 165 provided by Brugger at 23°C and under an oxygen flow of 80 ml/min, according to the standard ISO15165-1. Measurements at higher temperature (35 and 45°C) were also performed for studying a temperature range closer to the actual operating conditions of the PV devices.

IV.2.4 Accelerate ageing tests

All film samples have undergone an accelerate damp-heat ageing test at temperature of 85°C and relative humidity (RH) of 85% according to the standard IEC 61646:2008[10]. The active barrier properties and the optical properties (transparency) were periodically assessed during the ageing treatment of 5 days. Ageing tests were carried out with the climatic chamber CHALLENGE 250 (Angelantoni).

IV.2.5 Active-passive barrier layer lamination

The Poliprotect active PET film was laminated with a commercial PETSiOx film of 12 μm provided by AMCOR, composed of a polymer substrate (PET) with an inorganic coating (SiOx) layer of ~ 50 nm deposited using Electron Beam Evaporation.

---

[10] International Electrotechnical Commission Standard for Thin-film terrestrial photovoltaic (PV) modules - Design qualification and type approval

IV.3 Results and Discussion

Active and standard PET films were produced as specified in the experimental part and tested for their thermal and optical properties. The active PET film was also tested for its oxygen absorption performance.

IV.3.1 Thermal Characterization

The thermograms of Poliprotect, Novapet and P60 films are shown in Figure IV. 3a-c, respectively, while the assessed thermal parameters are reported in table IV.2.

A) I heating scan

B) Cooling scan

C) II heating scan
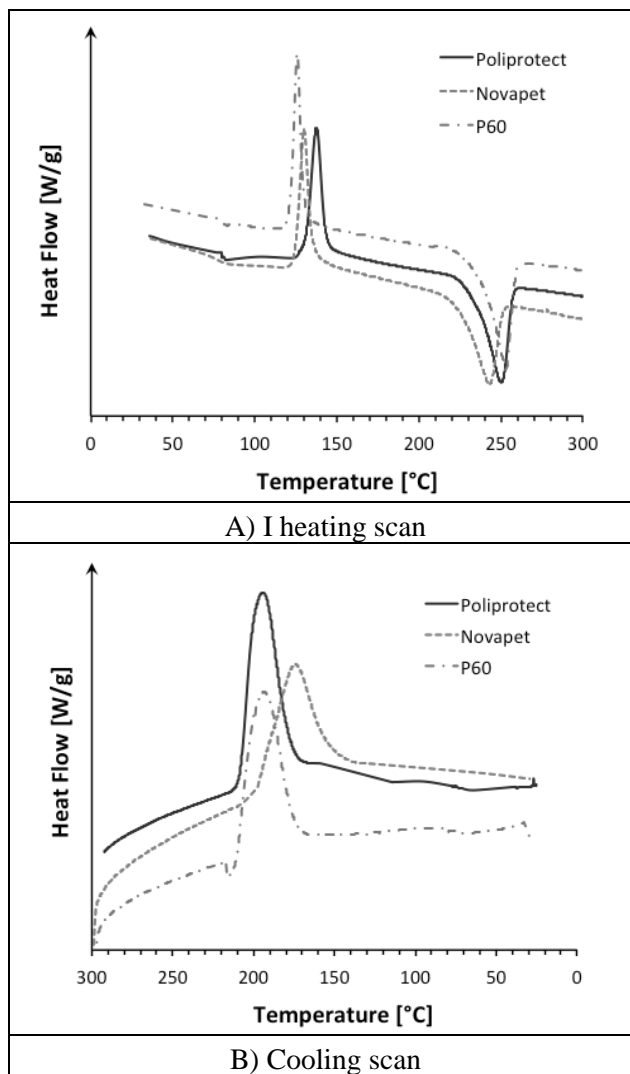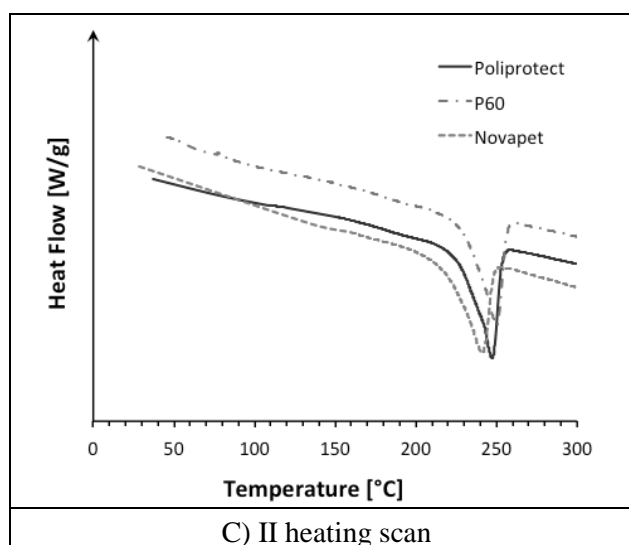
Figure IV.3 *DSC thermograms of Poliprotect, Novapet, and P60.*

Table IV.2 *Thermal Parameters evaluated in the DSC scans for the produced films of Novapet, P60 and Poliprotect.*

Polymer Sample	T_g [°C]	T_{cc} [°C]	ΔH_{cc} [J/g]	Tm_I [°C]	ΔHm_I [J/g]	Xc_I [%]	T_c [°C]	ΔH_c [J/g]	Tm_{II} [°C]	ΔHm_{II} [J/g]	Xc_{II} [%]
Poliprotect	79.5	137.6	32.2	248.7	42.2	7.4	194.3	42.3	247.2	37.0	27.4
Novapet	81.3	129.6	27.7	241.0	37.9	7.6	174.7	37.3	241.0	33.5	24.8
P60	79.5	125.9	27.4	252.4	44.2	12.4	194.3	40.9	249.8	36.9	27.3

The thermograms of the first heating scan (Fig. IV.3a) show small differences in the thermal response of the three films, which can be ascribed to the differences in terms of Inherent Viscosity (I.V.), and then of molecular weight, of the corresponding resins. P60 that has the lowest I.V. has also the highest cold crystallization capacity (lowest T_{cc}) being easier the crystallization of the shorter macromolecular chains. Novapet and Poliprotect have T_{cc} values progressively rising with the corresponding I.V. of the resin. By increasing the amount and the quality of the crystal phase, the melting temperature (Tm_I) and the melting heat (ΔHm_I) became greater.

As a result, the P60 film shows a crystallinity degree Xc_I (12.4%) higher than the Poliprotect and Novapet ones (7.4-7.6%).

62

The thermograms of the cooling scans show (Fig. IV.3b) that both P60 and Poliprotect crystallize from the melt state at higher temperatures, if compared to Novapet. This is predictable for P60 that has the lowest I.V., whereas for Poliprotect it can be explained as the result of a nucleating effect due to the cobalt catalyst contained in the resin. However, the ΔHc values of the three films are very near one each other.

As expected, on second heating (Fig. IV.3c) no cold crystallization phenomena occur in all cases; the melting temperatures (Tm_{II}) are comparable with those measured in the first heating, whereas the melting heat values (ΔHm_{II}) are always higher of the corresponding ΔHm_I ones, giving a crystallinity degree Xc_{II} in the range 24.8-27.4%.

IV.3.2 Optical Properties

The optical properties of the films, which are of primary importance for materials intended to coating PV devices, were assessed with measurements of transmittance in the UV-Vis range on film samples having thickness equal to 24±2 µm. The obtained spectra (Fig. IV.4) point out that the standard Novapet and P60 PET resins show a high transparency, near 90% on the 400–800 nm spectra range. This transparency decrease up to 80% for the Poliprotect, but it remains still acceptable for photovoltaic applications.

The lower transparency of Poliprotect, if compared to other standard PET, may be related to the presence of the active phase (i.e. Ultramid® X17 copolyamide and cobalt salt), as reported in literature for other PET systems containing polyamides (Hu et al. 2005).
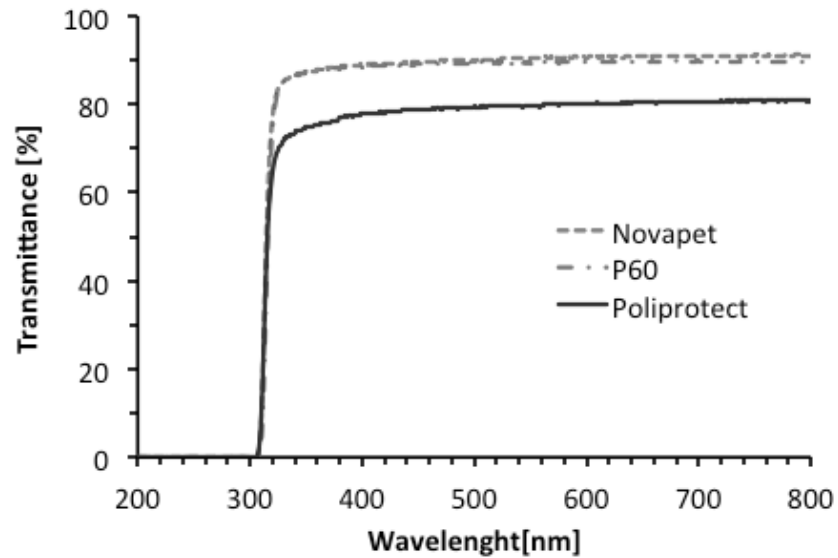
Figure IV.4 *Percent Transmittance of Novapet, P60 and Poliprotect in the UV-Visible range.*

In order to evaluate the effect of the heat on the optical properties of the films, UV-Vis spectra were also collected after accelerate ageing in damp-heat conditions (85°C, 85% R.H.) for different time intervals (24, 48 and 120 h).

The obtained curves are compared in Fig. IV.5a-c for Poliprotect, Novapet and P60, respectively.
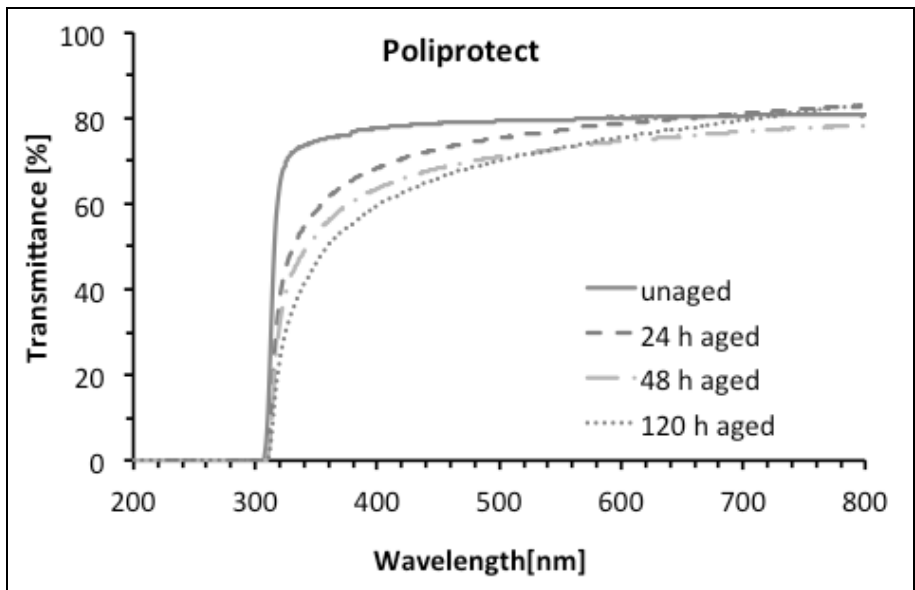
a)
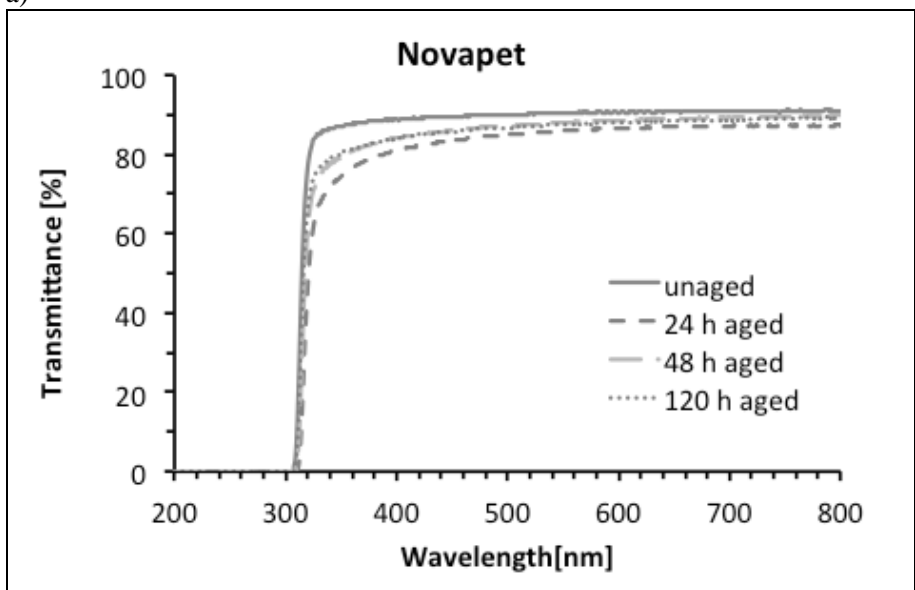
b)
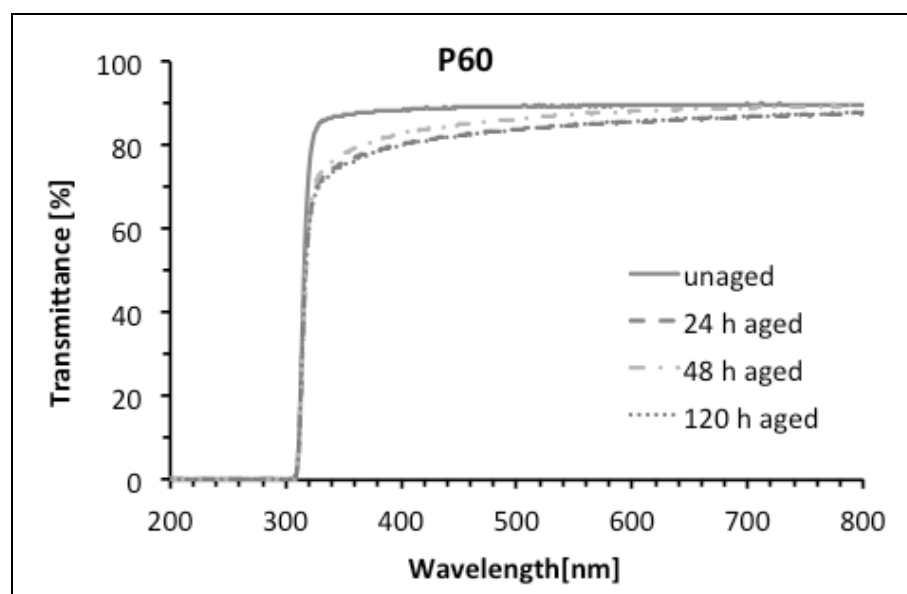
c)

Figure IV.5 *Effect of damp-heat ageing on the UV-Vis spectra of Poliprotect (a), Novapet (b) and P60 (c) films at different ageing times.*

The figures show that, after the ageing, all film samples maintain their transparency only at the longest wavelength, and become more opaque mainly in the wavelength range between 300-500 nm. The phenomenon can be ascribed to an increase in the film crystallinity at the damp-heat ageing test conditions. In these conditions, in fact, all the polymers can have enough molecular mobility to crystallize, due to the high temperature (T > Tg ~ 80°C, see Tab. IV.2) and high partial pressure of water vapor, which is a plasticizer for PET. The effect is particularly significant in the case of Poliprotect film, where the presence of cobalt salt can also catalyze some thermal degradation phenomena, as suggested by some literature findings that confirm the effects of transition metal ions on the thermal degradation of PET and various plastic materials (Fairgrieve 2009, Chiu and Cheng 2000).

IV.3.3 Oxygen Absorption Properties

With the aim to evaluate the oxygen absorption properties (i.e. oxygen-scavenging capacity, oxygen absorption rate, exhaustion time) of the Poliprotect active film, oxygen absorption measurements were performed in continuous as described in the experimental section.

66

The test were carried out at 25°C on both film samples with dry surface conditioned at indoor relative humidity and film samples with wet surface, in order to put in evidence possible effects due to different environmental exposure conditions. The results are reported in Figure IV.6.
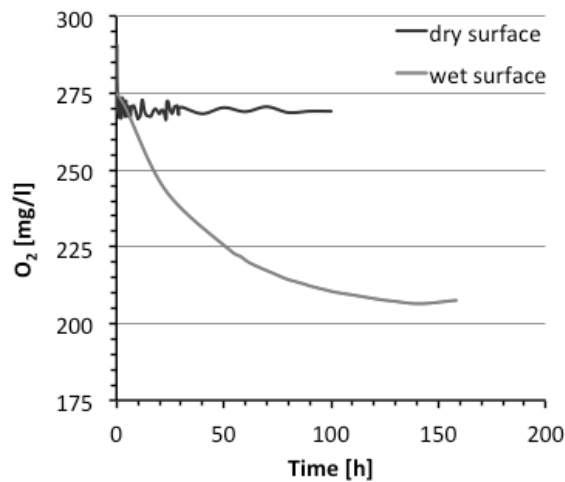
Figure IV.6 *Absorption oxygen kinetics at 25°C for Poliprotect samples in the following test conditions: dry surface and wet surface.*

It can be clearly observed that the oxygen absorption is activated by the water. In fact, the sample with dry surface does not show any detectable activity, while the sample with wet surface immediately reacts with the oxygen inside the test cell, giving a reduction of the O_2 concentration from ~ 48 ppm to ~ 36.5 ppm after 147 h, corresponding to the end of the sample's activity.

However, the Poliprotect film with dry surface, tested for its passive barrier properties to oxygen permeation, showed transport parameters comparable to that of the standard Novapet film, used for comparison, as it comes out from results of permeability experiments reported in Table IV.3.

Table IV.3 *Oxygen Barrier Properties of Poliprotect and Novapet at 23°C: diffusion coefficient D, sorption coefficient S, permeability P and gas transmission rate GTR.*

Film Sample	D [cm^2/s]	S [cm^3/cm^3 bar]	P [cm^{3}mm/m^{2}d bar]	GTR [cm^3/m^2 d bar]
Poliprotect	9.40·10^{-9}	7.38·10^{-2}	5.99	239
Novapet	5.28·10^{-9}	1.16·10^{-1}	5.29	203

In order to determine the O$_2$ absorption kinetics (i.e. the rate constant *k* and the order of reaction) of the film sample with wet surface, the natural logs (ln) of the experimental data of O$_2$ concentration measured in the vessel atmosphere at short times of test were plotted against time. If the ln plot approximated a straight line, the reaction was regarded as first order.

In general, the oxygen scavenging is a complex and heterogeneous process, involving the physical dissolution into the polymer, oxygen diffusing through the polymer and reaction of the polymer with oxygen (Gillen and Clough 1992, Rincon-Rubio et al. 2001). However, it was shown (Kevin et al. 2012) that for thin enough films, the rate of oxygen uptake is not limited by diffusion and the results can be analyzed by a simple kinetic model.

The reaction mechanism is based on the oxidation of copolyamide that is catalyzed by cobalt salt (Bacskai et al. 1997): the oxidation of the copolyamide units under the condition of interest involved rather complex chemistry, and the details of the reaction are beyond the scope and the interests of the current study. Furthermore, although the oxygen uptake is a heterogeneous process, in practice, for thin enough film, it may be considered as a homogeneous process.

A simple kinetic model is generally assumed for this kind of systems:

$$d[O_2]/dt = K[O_2]\,[OS] \qquad\qquad (IV.2)$$

where [O$_2$] and [OS] are the concentration of oxygen and of the reactive sites of the oxygen scavenger, respectively.

In case of catalytic scavengers without scavenger depletion, assuming in other words that there is a stoichiometric excess of the oxygen scavenger, [OS] may be considered constant and the equation above may be written as follows:

$$d[O_2]/dt = k[O_2] \qquad\qquad (IV.3)$$

This assumption may be reasonable in the first stage of the oxygen absorption phenomena.

Then, the equation above can be written as follows:

$$d[O_2]/ [O_2]= kdt \qquad\qquad (IV.4)$$

and then integrated:

$$\ln[O_2]_t= \ln [O_2]_{t=0}- kt \qquad\qquad (IV.5)$$

Rate-constants were calculated through a linear regression model by applying the ordinary least squares method using the eq. (IV.5), where $[O_2]_t$ is the amount of oxygen at time t (h), k the rate constant (h^{-1}), and $[O_2]_{t=0}$ the initial amount of oxygen.

The scavenging capacity of the active samples was evaluated by dividing the amount of oxygen, absorbed from the beginning of the test to the plateau value, by the film weight.

The exhaustion time (t_{LE}) was determined at the beginning of the plateau region, where the oxygen absorption is over.

All the values determined are reported in Table IV.4.

Table IV.4 *Constant of first-order kinetic equation, scavenging capacity and exhaustion time for Poliprotect films with wet surface, at 25°C.*

Constant of first-order kinetic equation			Exhaustion time	Scavenging capacity
k [h^{-1}]	$O_{2,t=0}$ [mg/l]	correlation coefficient R^2	[h]	[mg O_2/g film]
0.0035	271.7	0.98	147	6.97

In order to investigate the effect of higher amount of environmental water on the oxygen absorption capacity of Poliprotect, oxygen absorption measurements at 25°C were also performed immerging the film in liquid water and monitoring the reduction of the oxygen dissolved in water, as a function of the time.

Due to the small volume of the test vial and to the low amount of oxygen dissolved in water (8.3 mg/l at 25°C and 1 atm), compared to that contained in air (275 mg/l at 25°C and 1 atm), when immersed in water the Poliprotect film absorbed all the oxygen present in the vial without exhausting its action. Therefore, with the aim to follow the reaction kinetics for longer times, as

soon as the oxygen was exhausted, the test vial was discharged and refilled with fresh water, so as to reconstitute the initial O_2 level. This operation was repeated for three times, for a total test duration of approx. 1450 h (60 days). The obtained curve is reported in Fig. IV.7.

The experiment at short times was also performed at 35°C and 45°C, in order to evaluate the temperature effect on the oxygen absorption kinetics. The values of the constant of first-order kinetic equation were calculated according to eq. IV.5 and reported in Table IV.5.
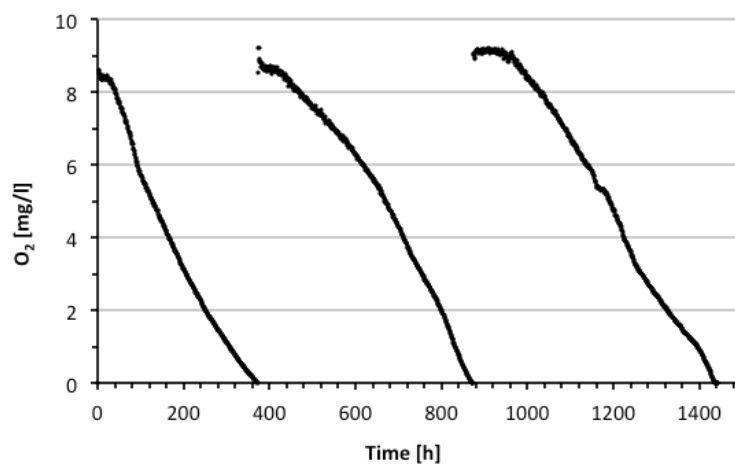
Figure IV.7 *Absorption oxygen kinetics at 25°C for Poliprotect samples immersed in water. The three curves correspond to three consecutive measurement runs on the same film sample, after discharging/refilling the test vial with fresh water, so as to reconstitute the initial O_2 level and to follow the reaction kinetics for longer times.*

As it can be seen, also in this test conditions the Poliprotect film does not exhaust neither after three runs. However, compared to the film with wet surface, the constants of first-order kinetic equation calculated at 25°C at short times (Tab. IV.5) demonstrated that the Poliprotect film reacts progressively faster with the oxygen with increasing the environmental humidity. Of course, the reaction kinetics becomes faster if the test temperature is increased.

70

Table IV.5 *Constants of first-order kinetic equation for Poliprotect films immersed in water, at 25°C, 35°C and 45°C.*

T	Constant of first-order kinetic equation		
[°C]	k [h^{-1}]	$O_{2,t=0}$ [mg/l]	correlation coefficient R^2
25	0.0132	8.49	0.98
35	0.2745	7.18	0.99
45	0.8797	6.40	0.99

IV.3.4 Active-Passive Barrier Bilayer

On the basis of the above results, a preliminary multilayer active-passive barrier structure (Fig. IV.8) was designed and prepared by lamination of the active barrier layer of *Poliprotect* with a passive barrier bilayer, PET-SiOx, which is a standard material employed for coating flexible solar cells.

FIGURE IV.8. *Scheme of the multilayer structure for the solar cell barrier encapsulant*

The optical properties of the multilayer structure were assessed and compared to that of the standard PET-SiOx standard bilayer (Fig. IV.9). A reduction of ~ 15% of transmittance was measured for the multilayer if compared with the PET-SiOx bilayer. The analysis of the oxygen barrier properties for the active-passive barrier multilayer is currently in progress.
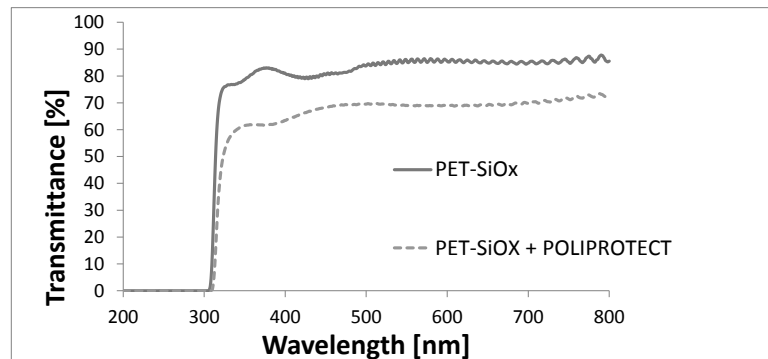
Figure IV.9 *% Transmittance in the UV-Visible range of samples: PET-SiOx and PET-SiOx + Poliprotect.*

IV. 4 Conclusions

The obtained results show that *Poliprotect* is potentially suitable for coating photovoltaic cells, since its absorption kinetics is slow and the O_2 barrier functionality is activated by changes in the environmental humidity due to meteorological phenomena (diurnal temperature variation, rain, etc.).

In addition, the produced *Poliprotect* film exhibits an acceptable transparency and is proven to be easily processable.

The preliminary multilayer active-passive barrier structure, developed laminating an active layer of *Poliprotect* with a passive PET-SiOx barrier film, also showed acceptable transparency.

Its oxygen barrier properties are now under scrutiny in view to test it on organic solar cells in order to assess its capability to preserve the efficiency of the PV devices during the time.

Chapter V
Multilayer Layer Coatings and Solar Cells Encapsulation – Preliminary Data

V.1 Introduction

In this chapter some preliminary characterization results are reported concerning the barrier and optical properties of several flexible multilayer structures that were developed. The multilayer coatings, together with other structures including the multibarrier layers developed in the previous research phase (see Chapter III), were applied to organic solar cells at lab scale at the Center for Nano-Science and Technology@PoliMi of the Fondazione Istituto Italiano di Tecnologia.

The efficiency evolution during the time is currently analyzed for the PV devices encapsulated with the flexible coatings and compared with the efficiency of PV devices encapsulated with glass.

Although the experimental work is still running, preliminary data are reported in the section V.4.3 of this chapter.

V.2 Experimental details

Multilayer structures were obtained by laminating single layer samples of PET-SiOx (12 μm thickness) and ETFE-SiOx (100 μm thickness), both provided by AMCOR[11] using the silicon adhesive "Pattex" (Henkel). Some multilayer structures were created including also the PET-SiOx nanocoated samples developed in the previous phase of this study (see chapter III), and

---

[11] www.amcor.com

specifically the sample FAS1 E, which showed best overall performance in terms of barrier properties to oxygen and water.

The multilayer structures composition and the associated identification code used in this chapter are reported in Tab. 5.1.

Table V.1 *Composition and identification codes of multilayer and single layer samples.*

Sample composition	Identification Code
1 layer PET-SiOx	1PETSiOx
2 layers of PETSiOx	2PETSiOx
5 layers of PETSiOx	5PETSiOx
8 layers of PETSiOx	8PETSiOx
1 layer of FAS1 E + 1 layer of PETSiOx	SAM + 2
1 layer of FAS 1 E	SAM
3 layers of PETSiOx 1 layer ETFESiOx	3PETSiOx + ETFESiOx

The transparency was evaluated by measuring the UV-visible transmittance of the obtained films from 200 nm to 800 nm with the UV-Visible Spectrophotomer λ 800 (Perkin Elmer).

The OTR (Oxygen Transmission Rate) measurements were carried out with the Permeabilimeter GDP – C 165 provided by Brugger at 23°C and under an oxygen flow of 80 ml/min according to the standard ISO15165-1.

Measurements at higher temperature (35°C and 45°C) were also performed for studying a temperature range closer to the actual operating conditions of the PV devices.

V.3 Results of Multilayer Characterization

V.3.1 Oxygen Barrier Properties

A comparison analysis of the oxygen barrier properties of the multilayer coatings with different number of layers was performed, and the obtained data are reported in Tab. V.2.

Table V.2 *Oxygen Transmission Rate of single layer and multilayer coatings*

Sample	OTR [cm^3/m^{2}d bar]
1PETSiOx	11.4
2PETSiOx	5.02
5PETSiOx	2.38
3PETSiOx+ETEFSiOx	0.92
8PETSiOx	0.46
SAM +2	0.84
SAM	3.8

It can be seen from tab. V.2 that the FAS nanocoated sample of PETSiOx (SAM) has higher barrier properties (3.8 cm^3/m^{2}d bar) if compared to the sample composed of 2 uncoated layers of PETSiOx (5.02 cm^3/m^{2}d bar). This is an interesting result demonstrating that a reduction of the number of the necessary layers for protecting the solar cells may be achieved using the multibarrier layers studied and developed in the previous research phase (see Chapter III), that was an objective of this PhD work (§ II.5).

In Fig. V.1 the Oxygen Transmission Rate is reported in function of the number of layers included in the multilayer structures. Clearly, the OTR decreases in function of the number of layers.
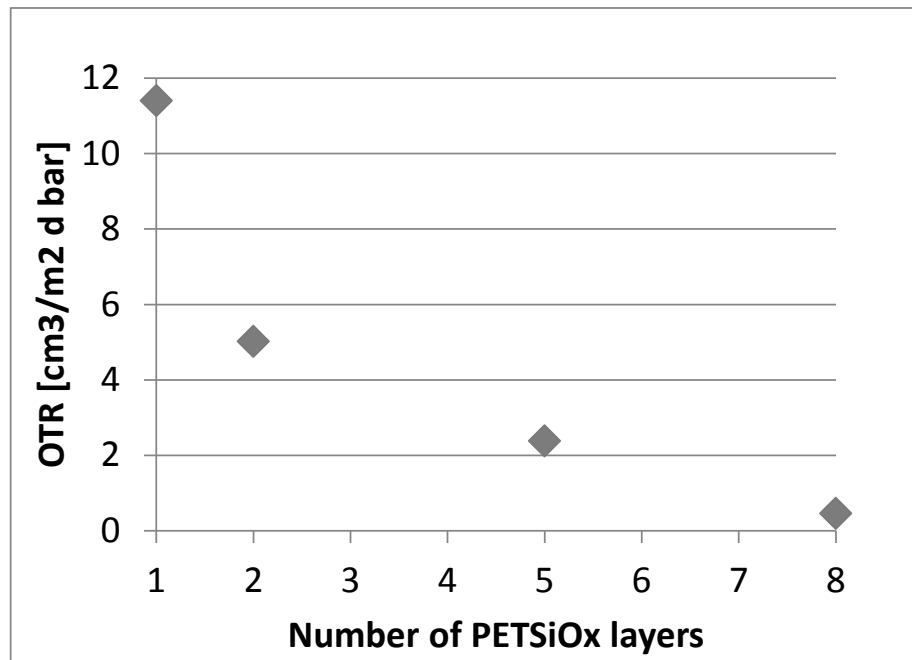
Figure V.1 *Oxygen Transmission Rate in function of the number of layers for the multilayer samples of PET-SiOx.*

V.3.2 Optical Properties

All the different multilayer structures were also investigated in the UV-Visible range in order to analyze their optical properties and the obtained spectra are shown in Fig. V.2. As expectable, the transparency significantly decreases at all wavelengths with the increase of the number of layer in the structure.
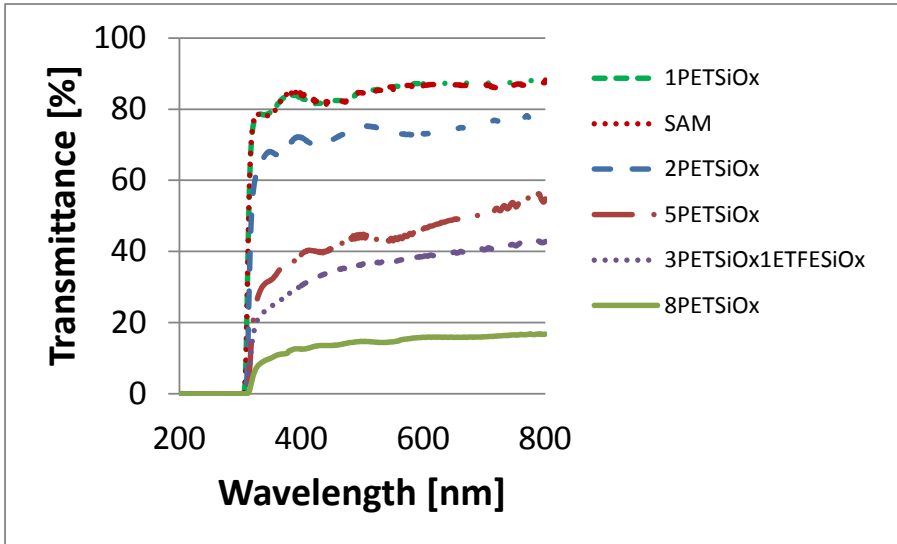
Figure V.2 *Percent transmittance of multilayer coatings of PETSiOx and ETFESiOx*

While the single layer and the bilayer structures have transmittance values acceptable for PV application as frontsheet, the other multilayers are too opaque for this application, but they may be suitable as backsheet or also for coating PV sensors, for which the stability is more important than sensitivity.

The multi-barrier layer (SAM) has the same transparency of the uncoated PETSiOx, as shown in figure above (see also Chapter III).

As already told in the previous section V.3.1, the use of the FAS coated PETSiOx allows to reach the same value of the oxygen barrier properties (see Tab. V.2) with approximately the half of the number of layer, and this may turn out to be useful also in terms of improved optical properties and, consequently, in terms of solar cells efficiency.

V.4 Application of the Multilayer Coatings to Organic Solar Cells

Some of the multilayer structures previously laminated were used to encapsulate organic PV devices at lab scale. The organic solar cells are bulk hetero-junction cells with fullerene as acceptor and a low-bandgap polymer as donor. The production process of the PV devices is shortly described in the following subsection V.4.1.

V.4.1 Organic Solar Cells production process at lab scale

The production process of solar cells at lab scale was based on the classical deposition method present in laboratory, and on a glass substrate.

The base substrate is a square-shaped slide of glass (about 1cmx1cm) which has already been covered with the electrode consisting of a layer of ITO (Indium Tin Oxyde).This substrate is cleaned thoroughly by repeated cycles of sonication in acetone and isopropanol, followed by an oxygen plasma treatment that concludes the process.

Thus, it is possible to start to build the cell on the top of this substrate by spin-coating. Then, a first layer is deposited which should facilitate electrons passage and/or block the holes. This layer has to be annealed on a hotplate.

Subsequently, the same technique is used to deposit the active layer. As this is a bulk hetero-junction cell, the active layer is composed by a blend of an electron donor and an electron acceptor material. Usually, this step is done inside a glove box where a nitrogen controlled atmosphere is maintained.

Finally, an electron blocking layer is deposited with the spin-coater and then the silver top electrode is evaporated. For this, the samples are aligned on a mask with the desired electrode pattern, and then the whole is put into the evaporator.

After evaporating, the samples are kept in the glove-box, and their metal legs are attached in contact with each of the electrodes.

Still in glove-box, the cells are encapsulated in order to protect them from oxygen degradation once outside of the glove-box. An epoxy resin is used on top of the cell, then closed with a small slide of glass or flexible coating layer.

The next section (§ V.4.2) provides further details on the encapsulation process.

V.4.2 Encapsulation of organic solar cells

The encapsulation of organic solar cells of dimensions 1.5 cm x 1.5 cm was carried out at the Center for Nano Science and Technology at the Fondazione Istituto Italiano di Tecnologia, in order to assess their effectiveness in protecting the cells and maintaining constant their efficiency during the time.

The multilayer coatings were applied on the solar cells with a bi-component adhesive provided by Robnor, composed by an epoxy hardener HX681C/NC and an epoxy resin RX681C/NC.

The following samples were used for encapsulating the organic solar cells: 1PETSiOx, 2PETSiOx, 5PETSiOx, 3PETSiOx1ETFESiOx, 8PETSiOx, SAM+1 (tab. V.1). Furthermore an additional multilayer

structure was laminated with 2 PETSiOx layers and 1 layer of the multibarrier layer obtained with the SAM of fluoroalkylsilanes deposited on the PET-SiOx (see chapter III). This last sample will be indicated from now on with the following identification code: SAM+2.

Approximately 50 samples were prepared and encapsulated with the flexible coating samples and subsequently stored in dark in-door environment. For comparison purpose, also reference samples encapsulated with glass were included in this preliminary study. Glass encapsulated devices were stored in the Glove Box under nitrogen atmosphere.

Figure V.3 *Organic Solar Cells in the Glove Box*

V.4.3 Characterization of the encapsulated PV devices

The encapsulated solar cells are stored in dark in-door environment and the current-voltage characteristics are measured periodically according to standard test method *ASTM G 173-03*, by exposing them to a commercial solar simulator Oriel Sol3A provided by NewPort. Electrical Measurements were performed with a Source Meter Unit Instrument model 2400 (Keithley), and included several pixels for each PV device.
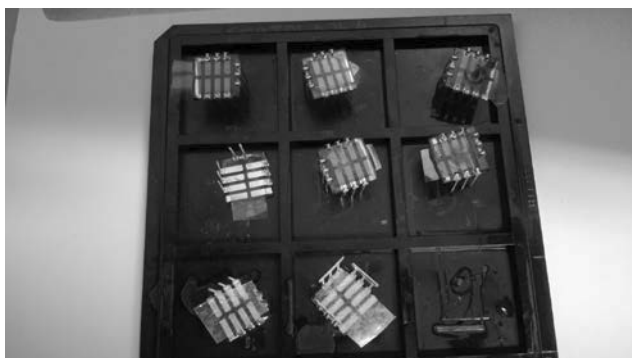
Figure V.4 *Organic Solar cells encapsulated with different multilayer structures*

Figure V.5 *I-V measurement for encapsulated solar cell exposed to solar simulator*

The I-V measurements are still running but encouraging data have been obtained at date. Preliminary results of power conversion efficiency (PCE) are reported in Table V.3 and in Fig. V.5.

Samples 8PETSiOx and 3PETSiOx1ETFEsiOx delaminated and thus the related data were not included in this preliminary analysis.

From Fig. V.5 some qualitative information may be obtained on the PCE

stability for the coated samples:

   - the reference sample in glass is the most stable during the time, as expectable,
   - the PCE trend of sample 5PETSiOx is more stable if compared to samples 1PETSiOx and 2PETSiOx PCE, and this is clearly a consequence of the higher barrier properties corresponding to the increased number of layers,
   - the multilayer structure that includes the layer of PETSiOx with the SAM nanocoating seems to be more effective than the other flexible multilayers, with a PCE stability that is comparable to that of the reference sample in glass.

Table V. 3 *Percent Power Conversion Efficiency of PV devices coated with flexible barrier coating compared to the glass coated reference sample (average values).*

| %PCE	1PETSiOx	2PETSiOx	5PETSiOx	SAM+1	SAM+2	GLASS
Initial value	3.13±0.91	3.48±0.22	3.27±1.2	4.00±1.38	4.20±1.00	4.05±1.98
After 33 days	3.06±1.15	2.54±0.40	3.44±1.24	4.11±1.46	3.77±1.79	4.03±1.91
After 71 days	2.86±1.00	2.05±0.44	3.90±1.34	3.79±1.56	3.22±1.84	n. a.

n.a.: not available
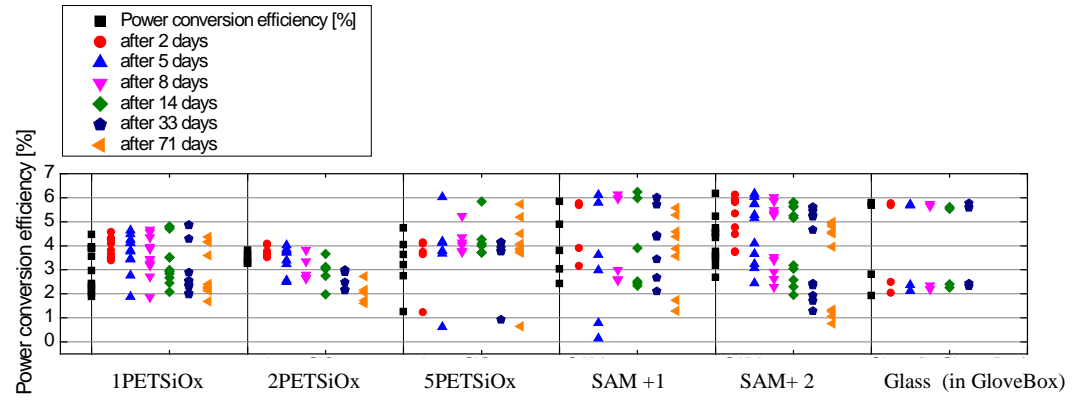
Figure V.6 *Percent Power Conversion Efficiency of solar cells encapsulated with flexible coatings and glass in function of the time.*

CONCLUSIONS

This Ph.D. study aims to develop new passive and active barrier materials for coating flexible solar cells in order to extend their lifetime.

In the first phase of the research, a method was studied able to enhance the barrier properties against the atmospheric degradation agents of the flexible coating layers usually employed for coating solar cells. A single step process carried out at room temperature was developed, allowing to modify a standard coating bilayer employed for solar cell application and significantly improve its liquid H_2O barrier properties (average CA > 130°), its oleophobic properties (average CA > 90°) and also the oxygen barrier properties of about 70%. The method was based on the Self-Assembly of Monolayer of hydrophobic molecules that are chemisorbed on the inorganic layer of the coating substrate. In this way, a passive multibarrier coating was produced, that integrates both liquid water barrier and oxygen barrier properties, allowing to reduce the number of necessary layers to protect the solar cells and preserve their efficiency during the time.

Subsequently, several multilayer structures of flexible barrier coatings were laminated and characterized. It was found that the multibarrier passive materials previously studied obtained allow to obtain the same barrier properties with approximately the half of the number of standard coating layers. Some of these multilayer were specifically designed and applied to encapsulate organic solar cells at lab scale, and encouraging results have been obtained. In particular, it was found that after more than 70 days the PV devices encapsulated with flexible bilayer coating composed by an uncoated PETSiOx layer laminated with a multibarrier layer have a power conversion efficiency that is comparable to that of reference PV devices encapsulated in glass and stored in Glove Box.

However, no significant difference was measured among the different multilayer structures and such aspect needs be better investigated with further analyses, also considering that the data on the current-voltage characteristics of the cells are still under collection.

Another phase of the PhD study was aimed to develop an active barrier coating for solar cells able to continuously adapt its protective action

according to the intensity of the environmental degradation phenomena. To this aim, suitable transparent polymer substrates including oxygen absorbers, were produced and characterized. The obtained results showed that the developed active films of PET are potentially suitable for coating photovoltaic cells, since their absorption kinetics is slow and the O_2 barrier functionality is activated by changes in the environmental humidity due to meteorological phenomena (diurnal temperature variation, rain, etc.). In addition, the produced active barrier system shows an acceptable transparency and is proven to be easily processable. The preliminary multilayer active-passive barrier structure, developed laminating an active layer with a passive PET-SiOx barrier film, showed acceptable transparency.

The coating materials studied and developed with the above approaches are thought to be included in a multilayer structure where they can act synergically in order to guarantee a better protection to the flexible solar cell, by strengthening the protective action of passive barrier layer with an active barrier one capable to react and adapt its protection to the environmental degradation phenomena.

Future research activities are planned in order to complete the study of the stability of the PV devices encapsulated with the flexible barrier layers, by optimizing the multilayers encapsulation procedures and investigating the effect of accelerate ageing on the encapsulated solar cells.

Furthermore, the study of the active barrier layers will be further deepened in in view to test them on organic solar cells for assessing their capability to preserve the efficiency of the PV devices during the time.

REFERENCES

Abenante, L. et al. Long-Term Performance Degradation of c-Si Photovoltaic Modules and Strings. *Proc. of 25th European Photovoltaic Solar Energy Conference*, 2010 Valencia, Spain; p. 4023–4026.

Altavilla, C. an Ciliberto, E. (2011) Surface Modification induced by Cleaning and Protective Treatments in Cultural Heritage Materials (an XPS Altavilla and Ciliberto Eds. Nova Sci. Publishers).

Amberg-Schwab, S. et al. (2006) Development of Passive and Active Barrier Coatings on the Basis of Inorganic–Organic Polymers. *Monatshefte fuer Chemie*, **137**, 657–666.

Avila, A. et al. (1999) *Atmospheric Environment,* **33** 1663-1667.

Bacskai, R. et al. (1997) Oxygen scavenging homogeneous modified Polyolefin-Oxidizable Polymer-Metal salt blends, US 5641827.

Bosco, N. and Kurtz S. (2010) Reliability concerns associated with PV technologies.

Brinker, C. J. (1988) *J. Non-Crys. Solids*, **100** 31-50.

Ching, G. C. et al., WO99/48963.

Chiu, S.-J. and Cheng, W.-H. (2000) *Journal of Analytical and Applied Pyrolysis,* **56**, 131–143.

Czanderna, A. W. and Pern F.J. (1996) *Sol. Energ. Mat. Sol. C.,* **43** 101-181.

Dhere, N.G. PV Module Durability in Hot and Dry Climate, *Proc. Of 16th European Photovoltaic Solar Energy Conference*, 2000.

Dhere, N.G. and Pandit, M.B. Study of Delamination in Acceleration Tested PV Modules, *Proc. Of 17th European Photovoltaic Solar Energy Conference*, 2001.

Erler, B. et al. Multilayer Materials for the Encapsulation of Thin Film Modules. *Proc. of 3rd World Conference on Photovoltaic Energy Conversion*, May 11-18 2003, Osaka, Japan.

Fairgrieve, S. (2009) Degradation and Stabilisation of Aromatic Polyesters, Published by iSmithers. Shawbury (UK) ISBN: 978-1-84735-457-0.

Frach, P. et al. (2008) *Surf. Coat. Tech.* **202** 5680-5683.

Galdi, M. R. and Incarnato, L. (2011). *Packaging Technology and Science*, **24**, 0894-3214.

Garcia, P. et al. (2010) Permeation measurements and modeling of highly defective Al_2O_3 thin films grown by atomic layer deposition on polymers", *Applied Physics Letters* **97**, 221901.

Garcia, P. et al (2010) Encapsulation of $Cu(InGa)Se_2$ Solar Cells with ALD Al_2O_3 Flexible Thin-Film Moisture Barrier: Stability under 1000 hour Damp Heat and UV Exposure" 978-1-4244-5892-9/10

Gillen, K.T. and Clough, R.L. (1992) *Polymer*, **33**(20):4358-65.

Glaves, S. et al.(2002) *Atmospheric Environment,* **36**, 3089-3099.

Goetzberger, A. et al. (2003) *Materials Science and Engineering* **40**, 1 – 46.

Gouesbet, G. and G. Gréhan, G. (2011) Generalized Lorenz-Mie Theories, Springer, Berlin Heidelberg, 978-3-642-17193-2978-3-642-17193-2.

Haas, K.-H. et al. (1999) Functionalized coatings based on inorganic–organic polymers (ORMOCER®s) and their combination with vapour deposited inorganic thin films. *Surface and Coatings Technology*, **111,** 72–79.

Hammond, R. et al. *Proc. of the 26th IEEE PVSC 1997.*

Hu, Y. S. et al. (2005) Improving transparency of stretched PET/MXD6 blends by modifying PET with isophthlate. *Polymer* **46**, 5202–5210.

86

Ichimura et al. (2012) Patent GB24489990A.

G. J. Jorgensen et al. (2006) *Solar Energy Materials & Solar Cells*, **90**, 2739–2775.

Karunakaran, R. G. et al. (2011) *Langmuir*, **27**, 4594–4602.

Kevin, K. et al. (2012) *Polymer* **53,** 4211-4221.

King, D.L. et al. Stabilization and Performance Characteristics of Commercial Amorphous-Silicon PV Modules, *Proc. of 28th IEEE PVSC* 2000, pp. 1446-1449.

Knock, U. and Zachmann, G. (1996) *Macromolecules*, **29** p. 6019.

Krebs, F. C. and Norrman, K.(2007) Analysis of the Failure Mechanism for a Stable Organic Photovoltaic During 10 000h of Testing, *Prog. Photovolt: Res. Appl.***15**, 697–712.

Langereis, E. et al. (2006), *Appl. Phys. Lett.* **89** 081915.

Ling, X. Y. et al. (2009) Stable and Transparent Superhydrophobic Nanoparticle Films. *Langmuir,* **25**, 3260 – 3263.

Logothetidis, S. et al. (2010) *Eur. Phys. J. Appl. Phys.* **51**, 33203.

Lu, X. et al. (2011) *Surf. Coat. Tech.* **206**, 1490-1494.

Lungenschmieda, C. et al. Flexible Encapsulation for Organic Solar Cells. Proc. of SPIE Vol. 6197, 619712, (2006).

Matthews, A. and Depree, C. US 6254804, 2001.

Maydannik P. S. et al. (2011) An atomic layer deposition process for moving flexible substrates", *Chemical Engineering Journal* **171** 345–349.

McConnell, et al. (2009) *Macromolecules* **42** 517–523.

McNaught A.D. et al. IUPAC Compendium of Chemical Terminology, 0-9678550-9-8, 2006.

Morlier, A. et al. (2013) *Sol. Energy Mater. Sol. Cells* **115** 93–99.

Oh, T. and C. K. Choi,C. K. (2010) *J. Korean Phys. Soc*. **56** (4), 1150-1155.
87

Olsen, L. Damp Heat Effects on CIGSS and CdTe Cells- Pacific Northwest National Laboratory.

Ozsoy, T. and Cemel Saydam A. (2000) *The Science of the Total Environment* **253**, 93-109.

Quintana, M. A. et al. Commonly observed degradation in field –aged photovoltaic modules. Proc. of Photovoltaic Specialists Conference, 2002.

Ravens, D. A. S. (1960) *Polymer*, **1** 375 – 383.

Ravichandran, J. et al. (2008) A novel polymer nanotube composite for photovoltaic packaging applications. *Nanotechnology* 19 085712 (5pp).

Reitze, A.J. ISBN 1-5876-027-7, chapt. 9. (2001).

Rincon-Rubio, LM, et al. (2001) *J. Polymer Degradation and Stability*, **74**(1): 177-88.

Rooney, M. L. Active Food Packaging , Blackie Academic & Prof., 1995.

Rossi G. et al. (2014) *Surface & Coatings Technology* **239**, 200–205.

Saitoh, T. et al. (2000) Overview of Light Degradation Research on Crystalline Silicon Solar, *Progress in Photovoltaics: Research and Applications,* DOI: 10.1002/1099-159X.

Sichina, W. *J.DSC as Problem Solving Tool: Measurement of percent crystallinity of thermoplastics thermal analysis, application note*.

Scheirs, J. (2000) Compositional and Failure Analysis of Polymers – A Practical Approach, ISBN 0471 625728 (Wiley).

Silicone Compounds Register and Review, Petrarch Systems, 1987

Teshima, et al. (2003), *Langmuir* **19**, 8331–8334.

Vaško, K. et al. (2009), *Cent. Eur. J. Phys.* **7** (2), 371–378.

Visser, R. J. *Printed Electronic*s 2008 USA.

Wronski, C.R. Amorphous Silicon Photovoltaics: Order from Disorder, *Proc. of 28th IEEE PVSC 2000*, pp. 1-6.

Xiu, Y. et al. (2008) Langmuir **24**, 10421–10426.